Volume 2
Number 13
7 July 2021
Pages 4105–4434

Materials Advances

rsc.li/materials-advances

ISSN 2633-5409

ROYAL SOCIETY OF CHEMISTRY

REVIEW ARTICLE

Maryam Sadat Kiai, Annapurna Nowduri *et al.*
History and recent developments in divergent electrolytes towards high-efficiency lithium–sulfur batteries – a review

Materials Advances

ROYAL SOCIETY OF CHEMISTRY

REVIEW

View Article Online
View Journal | View Issue

Cite this: *Mater. Adv.*, 2021, **2**, 4115

History and recent developments in divergent electrolytes towards high-efficiency lithium–sulfur batteries – a review

Srikanth Ponnada, [a] Maryam Sadat Kiai, *[b] Demudu Babu Gorle [c] and Annapurna Nowduri *[a]

Lithium–sulfur batteries, with a high specific capacity, low cost and environmental friendliness, could be investigated as a next-generation energy-storage system. However, the limitations of lithium–sulfur batteries in capacity retention are directly related to the role of the electrolyte. Recently, most of the research has focused on controlling the solubility of polysulfides in the electrolyte to minimize capacity fading. A range of electrolytes with much improved charge–discharge behavior has been suggested, for example, carbonates, ethers, ionic liquids and solid polymers as solid inorganic and novel hybrid electrolytes. Understanding real interactions with these improved electrolytes could lead to performance enhancement up to the levels of reliability needed for practical applications. In fact, the successful development of the lithium–sulfur battery needs a judicious choice of modified electrolyte. Additionally, the electrolyte composition should have good compatibility with the lithium anode as well as the cathode material. This review highlights the recent research progress for lithium–sulfur batteries with various improved electrolytes, with a focus on the chemistry of polysulfides, including polysulfide solubility and its influence on battery performance.

Received 10th April 2021,
Accepted 20th May 2021

DOI: 10.1039/d1ma00332a

rsc.li/materials-advances

[a] *Department of Engineering Chemistry, Andhra University College of Engineering (A), Andhra University, Visakhapatnam-530003, India. E-mail: dr.nannapurna@andhrauniversity.edu.in*
[b] *Nano-Science and Nano-Engineering Program, Graduate School of Science, Engineering and Technology, Istanbul Technical University, Istanbul, 34469, Turkey. E-mail: maryamskiai@gmail.com*
[c] *Materials Research Centre, Indian Institute of Science, Bengaluru-560012, India*

Srikanth Ponnada

Srikanth Ponnada has received his Dual Degree Integrated Masters in Applied Chemistry, Department of Engineering Chemistry from Andhra University College of Engineering-India having more than seven years of research and teaching experience, PhD research fellow in the field of "Functional Materials and it's Electrochemical Applications" at Department of Engineering Chemistry, Andhra University College of Engineering-India, his current research area includes Energy storage, Energy Conversion devices, Electrochemical Biosensors, Functional Nano Materials Synthesis and Metal organic frame works. Previously worked in CSIR-Central Electrochemical Research Institute, Karaikudi, Tamilnadu-India as a Project Scientific Assistant Grade-III in perovskite synthesis and application in photovoltaics and in IIT(ISM) Dhanbad-India as Project Junior Research Fellow in Gold Nanoparticle assisted heterogeneous catalysis.

Maryam Sadat Kiai

Dr Maryam Sadat Kiai has obtained her Master's degree in Energy System Engineering from The University of Manchester, England. She received her PhD with honors in Nano Science and Nano Engineering from Istanbul Technical University (ITU, Turkey) in 2020. She is working as a researcher in the microfluidics & microsystems laboratory of Istanbul Technical University. The nature of her PhD degree involved a great deal of research on nanofabrication techniques for the next generation of rechargeable batteries to improve energy storage capacity and electrochemical performance of rechargeable batteries. Her research expertise spans the fields of micro/nanofluidic systems, MEMS, thin film coatings, sensors and energy storage devices.

1. Introduction

Li-Ion batteries have been used for the past two decades in the battery market for portable electronic devices. Conventional Li-ion batteries with a graphite anode and a lithium transition-metal oxide cathode have low energy densities (theoretically, 350–400 W h kg^{-1}), which cannot satisfy market demands in addition to their high cost. Therefore, as the need for the development of compact and lightweight rechargeable batteries with a long cycle life increases, Li–S batteries with elemental sulfur cathodes and a high theoretical specific capacity of 1672 mA h g^{-1} are promising candidates. A sulfur cathode integrated with a Li metal anode could deliver the theoretical energy density of 2600 W h kg^{-1}, which is far greater than those of conventional commercial Li-ion batteries.[1–3] The naturally abundant, low-cost, and environmentally friendly sulfur cathode could persuade investors to commercialize lithium sulfur (Li–S) batteries. There are, however, some drawbacks with Li–S batteries, which have limited their market application, including (1) the insoluble and insulating nature of sulfur and polysulfide products, (2) the dendrites that form on the surface of the Li anode during cycling, causing capacity fading, (3) the large volume changes during cycling due to several redox reactions, which induce mechanical damage and (4) the dissolution of polysulfide in the electrolyte and active material transferring to the anode side. The dissolution and diffusion of soluble lithium polysulfides, as well as their migration toward the anode, are the most significant challenges, and result in the loss of active materials from the cathode, poor stability, and severe capacity fading. Various suggestions have been proposed to solve these problems. Most studies have been focused on nanostructured host materials such as porous carbons (nanotubes, nanofibres, and spheres),[4–9] graphene,[10–13] graphene oxide,[14–16] conductive polymers[17–21] and inorganic nanomaterials.[22–24] The conducting porous cathode hosts could enhance the electronic conductivity and confine polysulfides within their framework, subsequently improving the discharge capacity.[25–28] However, the electrolyte improvement still needs to be investigated exclusively for the high utilization of active materials. In fact, the approach, which focuses on electrolyte modification, seems to be effective. Various optimization approaches have been studied for the electrolytes, including the use of different solvents, salts, and additives, and even by applying solid electrolytes to restrain polysulfide shuttling. Consequently, it has been a major aim for electrolytes to control the transport of polysulfides through the cell. As a result, the electrolyte solutions have been found to be pivotal to the electrochemical performance of Li–S cells *via* analyzing the migration of polysulfides through the cell. Here, the most recent articles are studied on recent advances in electrolytes for Li–S batteries.

2. Electrolytes of lithium–sulfur batteries

Li–S batteries with a composite cathode and modified separator have been investigated recently, but only a few of these studies have focused on the role of electrolyte improvement for high-performance Li–S batteries. Electrolytes with a high ionic conductivity, stability, safe chemical reactivity and a high affinity with the cell component could play an important role in enhancing the performance of the batteries. Low solubility is considered as another important factor for electrolyte selection to hinder polysulfide migration and the shuttle effect. Additionally, the high potential of ion transport of an electrolyte could accelerate redox reactions for high-rate Li–S batteries. Fig. 1 shows a schematic of the Li–S cell with a liquid electrolyte.

Demudu Babu Gorle

Dr Demudu Babu Gorle is a Dr D. S. Kothari Postdoctoral Fellow in Prof. Karuna Kar Nanda's group in the Department of Materials Research Centre, Indian Institute of Science, Bangalore, India. His current research interests are focused on the rational design of advanced Metal–Organic Framework-based catalysts for Zn–air battery and fuel cell applications. He received his PhD degree in Chemistry from CSIR-Central Electrochemical Research Institute, Karaikudi, Tamil Nadu, India. He is focusing on developing an efficient catalyst for electrochemical energy conversion and sensor applications.

Annapurna Nowduri

Dr Annapurna Nowduri is presently an Associate Professor at Department of Engineering Chemistry, Andhra University College of Engineering, Andhra University, Visakhapatnam-India. She obtained her PhD (Best Thesis) in 2008 from Andhra University and has a teaching and research experience of more than 20 years. Her research interests are Chemical Kinetics, Li-ion Batteries, Electrochemical Sensors and Materials Synthesis. 15 PhD and 3 MPhil Degrees were awarded under her supervision. 63 research publications of national and international repute are in her credit. She has presented more than fifty papers in various national and international conferences. She served as reviewer/editorial member for various journals of national and international repute.

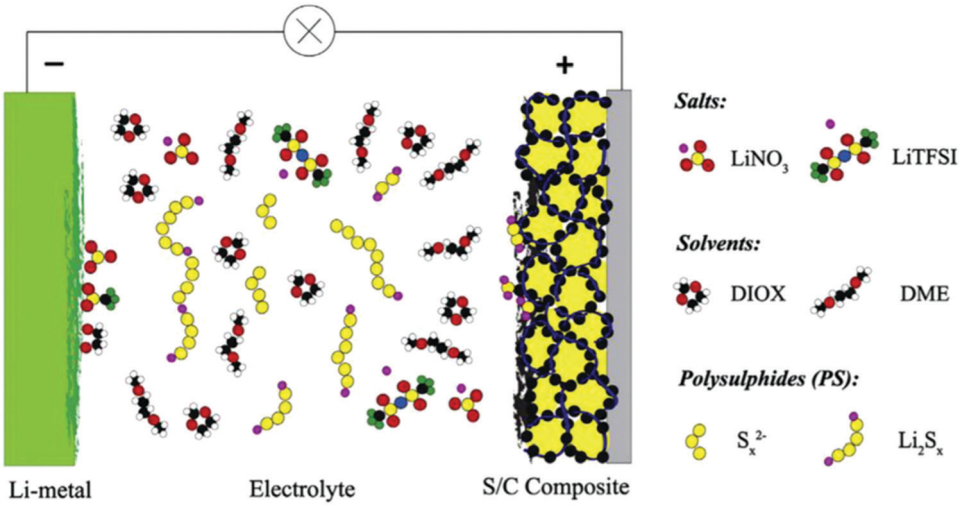

Fig. 1 Schematic of the components of a state-of-the-art Li/S battery with an electrolyte consisting of LiTFSI in a 1 : 1 mixture of DME and DIOX. Image reprinted with the permission from ref. 29. Copyright © 2014, Elsevier License-5041171085878.

The electrolyte's most important functions in a Li/S cell are ion transport between the electrodes and high chemical and electrochemical stabilities, which are also required for a high-rate Li–S battery. Migration of highly reduced species, which could react with the S_x^{2-} from the electrolyte, leads to the formation of lower order polysulfides (S_{x-n}^{2-}). On diffusing back to the cathode, these species are then re-oxidized into S_x^{2-}. The known redox shuttle influences both the discharge capacity and the efficiency of recharging.[29]

Electrolytes which have been investigated so far in all Li–S batteries are classified as liquid electrolytes, solid-state electrolytes, gel polymer electrolytes, ionic electrolytes, and novel electrolytes. The concentration of dissolved polysulfides (as Li_2S_x) can exceed 10 M in liquid electrolytes like ether-based electrolytes. Electrolytes with a high polysulfide concentration could provide an impressive capability for high-rated Li–S batteries as well as eliminating the problems associated with solid sulfur. The control of the behavior of polysulfides in solution should be investigated in all liquid electrolytes. In the past decade, in addition to working with liquid electrolyte solutions, several groups have studied solid electrolytes in a viable Li–S battery. Developing safe and high-ionic-conductivity electrolytes with novel additives could enhance the cycle life and increase hope for the commercialization of Li–S batteries.[30–33]

3. Liquid electrolytes

3.1 Carbonate solvents

Carbonate solvents such as ethylene carbonate (EC), diethyl carbonate (DEC), propylene carbonate (PC) and dimethyl carbonate (DMC) are commonly used in Li–S batteries. They provide high ionic conductivity and electrochemical stability. However, because carbonates can react with soluble polysulfides, the loss of active sulfur further leads to severe capacity fading of Li–S batteries.[34,35] However, integration of carbonate-based electrolytes with confined sulfur cathodes[36–42] or polymeric composite cathodes has shown an enhancement of the discharge capacity.[43–48] To illustrate the effect of a polymeric sulfur cathode with a carbonate electrolyte, He *et al.* suggested the sulfurized polyacrylonitrile (SPAN) cathode in a carbonate-based electrolyte. The SPAN composite with a sulfur content of 42.0% displayed the best electrochemical performance, with an initial capacity of over 700 mA h g^{-1}, and a capacity retention of over 97% after 80 cycles in the 1 M electrolyte $LiPF_6$/EC + DEC[49] (Fig. 2). A new desolvated gel electrolyte (DGE) is also being investigated to overcome capacity fading in Li–S batteries with the S-PAN cathode. The impedance plot obviously demonstrates a much smaller semicircle under the DGE than for the common electrolyte, and the charge-transfer resistance is reduced from 80 Ω for the common electrolyte to 27 Ω for the DGE[50] (Fig. 3).

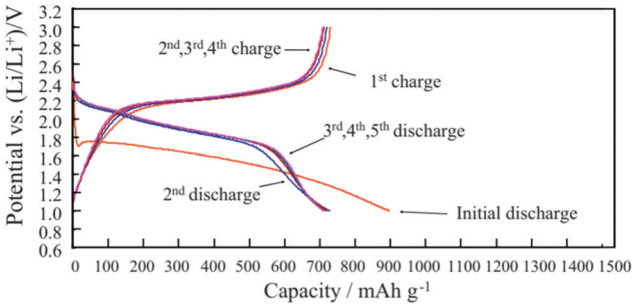

Fig. 2 Charge/discharge performance of SPAN cathode in 1 M $LiPF_6$/EC + DEC. Image reprinted with the permission from ref. 49. Copyright © 2012, Elsevier License 5041181200155.

3.2 Ether electrolytes

The most famous electrolytes in Li–S batteries are ether electrolytes, which can be operated in Li–S batteries at relatively low potentials (<3 V) and are much more stable than carbonates.

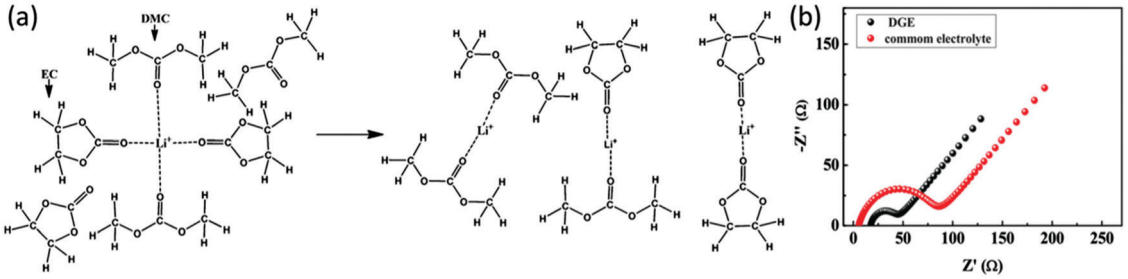

Fig. 3 (a) Schematic diagram of the solvation of Li ions in common electrolyte and concentrated desolvated gel electrolyte (DGE) and (b) impedance plots of Li–S cells with DGE and common electrolyte after the third cycle. Image reprinted with the permission from ref. 50. Copyright © 2014, American Chemical Society.

They include both linear and cyclic polymeric ethers such as 1,2-dimethoxyethane/1,3-dioxolane (DME/DOL),[51,52] tetraethylene glycol dimethyl ether (TEGDME),[53–56] tri(ethylene glycol)-dimethyl ether (TREGDME), diglyme (DGM or G3), and poly(ethylene glycol)dimethyl ether (PEGDME).[57,58] Ether-based electrolytes have a high stability toward polysulfides, a high donor number and a high conductivity with low viscosity, which could be applicable for all cathodes in Li–S batteries. The compositions of ether-based electrolytes need to be optimized to achieve high performance and long cycle-life Li–S batteries. Key parameters include the viscosity, conductivity, electrochemical stability, and safety. In recent studies on high-rate Li–S batteries, an electrolyte with a mixture of DME and DOL (1 M lithium bis(trifluoromethanesulfonyl)imide (LiTFSI) in DOL/DME (1 : 1 v/v)) has been investigated. These common ether electrolyte mixtures exhibit low viscosity, high conductivity, high polysulfide solubility, and satisfactory safety.

Additionally, developing an electrolyte that not only protects the Li anode from constant side reactions but also avoids the dissolution of PS from the cathode is a top priority. Since both PS solubility and reactivity to metallic lithium decrease when the molecular polarity of the ether solvent decreases, the solvent dibutyl ether (DBE) with a strong dielectric constant, low saturated vapor pressure, and viscosity is wisely chosen.[59,60] In another study, an ether-based electrolyte of 4 M LiFSI/DBE is proposed for Li–S cell which essentially hinders the dissolution of PS.

The dissolvability of Li_2S_6 in DBE and standard ether solvents (DME, DME/DOL, and TEGDME) used in Li–S batteries is seen in Fig. 4. The yellow sediment retained the Li_2S and sulfur mixture state. After stirring, the color of the three control groups changed to a dark red-brown colour. The observed phenomenon points to a clear inhibition of PS dissolution in DBE. It remains colorless after standing for more than 50 days, demonstrating DBE's efficacy for avoiding PS dissolution and reaction. Density functional theory (DFT) was used to measure the molecular orbital energies of DBE and LiFSI in order to further explain the SEI-forming mechanism at the molecular level.

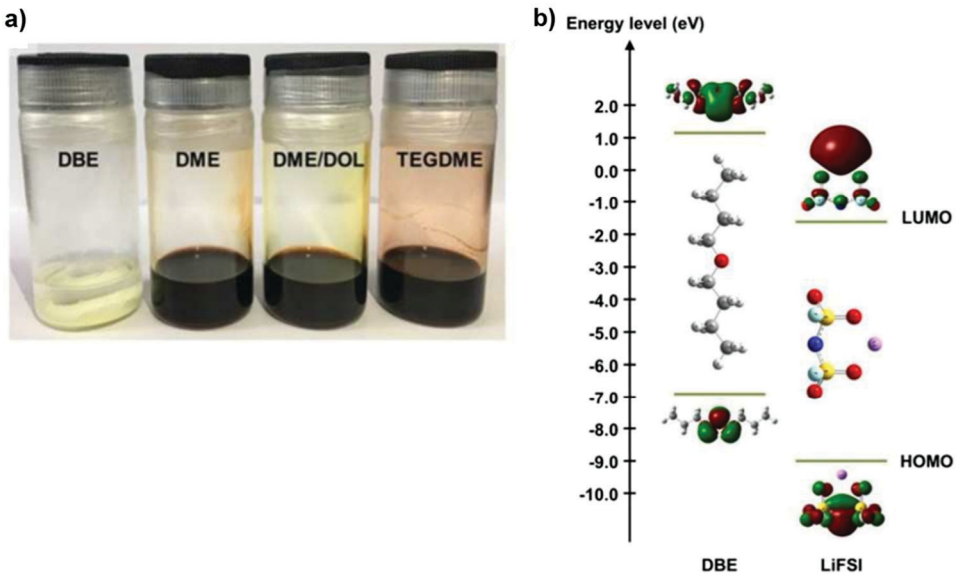

Fig. 4 (a) Photograph of dissolution test of 0.25 M Li_2S_6 in typical ether solvents by stirring stoichiometric amounts of Li_2S and sulfur in the solvents for 24 h. (b) The LUMO and HOMO energy values of DBE and LiFSI obtained by DFT simulations. Image reprinted with the permission from ref. 61. Copyright © 2018, Royal Society of Chemistry License-1117493-1.

On the surface of Li metal, LiFSI with a lower LUMO energy (−1.61 eV) is simpler to minimize than DBE (1.15 eV). As the salt concentration is increased to 4 M for the low molar ratio of DBE/LiFSI, the preferential reduction of FSI^- by Li metal is greatly improved.[61]

Several attempts have been made to introduce fluorinated ethers as solvents, including 1,1,2,2-tetrafluoroethyl-2,2,3,3-tetrafluoropropyl ether (TTE) and 1,2-(1,1,2,2-tetrafluoroethoxy)ethane (TFEE).[62–67] Recently a mixed diisopropyl ether (DIPE)-based electrolyte was proposed to shield the Li metal anode. The solubility of Li salts in DIPE is sufficient to provide the necessary ionic conductivity, while LiPSs are difficult to dissolve in DIPE.[68] As shown in Fig. 5, the deposited Li with the mixed-DIPE electrolyte showed compact and large area after 50 cycles. In the case of the EC/DEC and DOL/DME electrolytes, however, distinct Li dendrites can be seen. The mixed-DIPE electrolyte is advantageous for suppressing Li dendrite growth and thus ensuring long-term cycling of the cell. After 50 cycles, the Li metal anode thickness with the mixed-DIPE electrolyte increased from 50 to 77 μm, with dead Li accounting for 27 μm. The Li metal anode in the EC/DEC electrolyte, on the other hand, experienced significant volume expansion after cycling, to a thickness of 132 μm.

3.3 Ionic-liquid-based electrolytes (ILs)

Scientists have been drawn to high-performance Li–S batteries by ionic-liquid-electrolytes with low flammability, high stability, high conductivity, and a wide electrochemical potential window.[69,70] *N*-Methyl-*N*-butyl-piperidinium (PP14) bis(trifluoromethanesulfonyl)imide (TFSI) was considered as the IL electrolyte because of its acceptable electrochemical stability and suppressed shuttle effect. A comparison of the cycling performance of two different cells (Fig. 6) indicated that the use of the IL electrolyte can not only enhance the discharge capacity but also the cycling stability of the sulfur cathode.[71]

The cell using the PP14-RTIL demonstrated a high reversible potential of 1055 mA h g^{-1}, corresponding to a 63% sulfur consumption. The reversible capacity of sulfur can be stabilized at about 750 mA h g^{-1} after a few cycles, demonstrating sulfur's greatly improved cyclability compared with conventional liquid-electrolyte Li/S cells. The suppressed dissolution of polysulfides in the RTIL electrolyte tends to maintain the sulfur

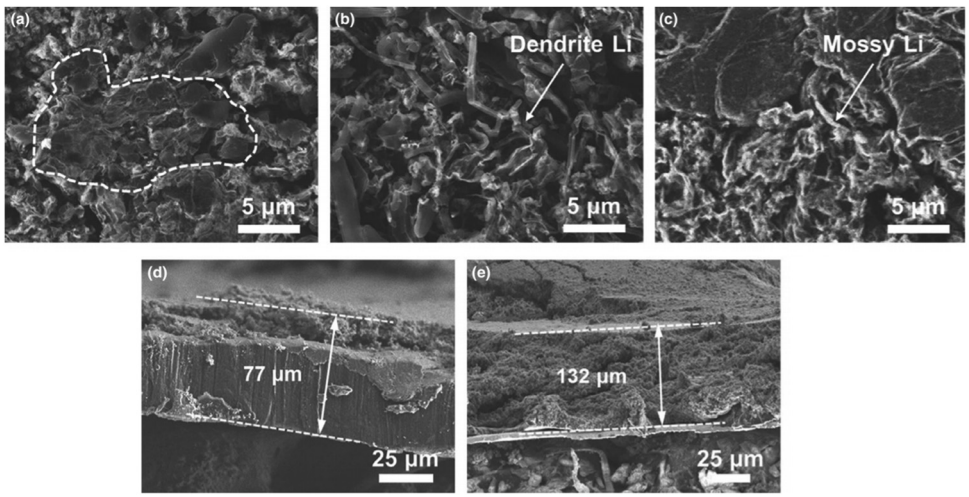

Fig. 5 SEM images of cycled Li anodes in Li|SPAN full cells after 50 cycles at 0.5 C with (a) mixed-DIPE, (b) EC/DEC and (c) DOL/DME electrolytes. The corresponding cross-sectional SEM images of the Li foils with (d) mixed-DIPE and (e) EC/DEC. Image reprinted with the permission from ref. 68. Copyright © 2020, John Wiley and Sons License 5064250079974.

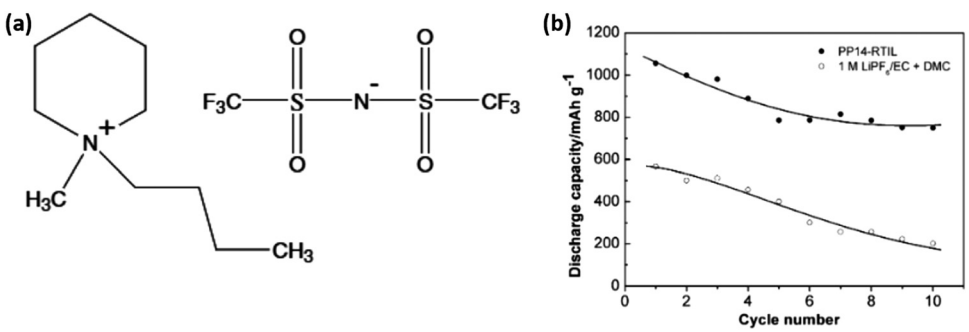

Fig. 6 Comparison of the cycling capacity of Li/S cells in (a) the IL electrolyte and (b) 1 M $LiPF_6$/EC + DMC. Image reprinted with the permission from ref. 71. Copyright © 2006, Elsevier License 5041350380913.

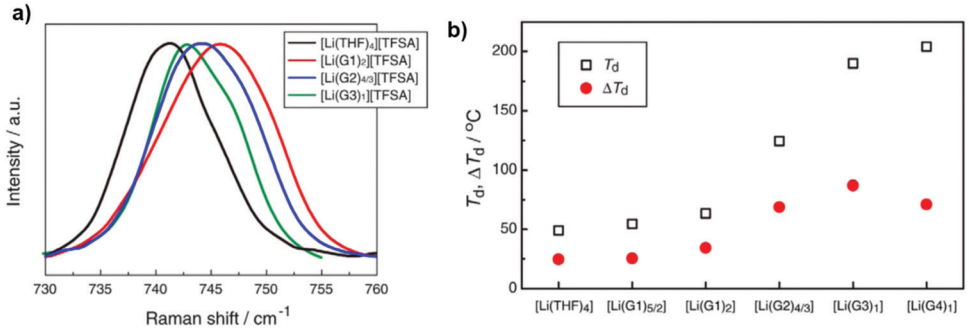

Fig. 7 (a) Raman spectra of [Li(glyme or THF)$_x$][TFSA] mixtures. (b) Thermal decomposition temperature (T_d) and its difference (ΔT_d) from T_d of the pure solvents of [Li(glyme or THF)$_x$][TFSA] mixtures. Image reprinted with the permission from ref. 72. Copyright © 2013, Elsevier License 5041350752944.

cathode's chemical composition and structure during charge–discharge cycles.

A new class of ionic liquids (ILs) was investigated recently through binary mixtures of lithium bis(trifluoromethanesulfonyl)amide (Li[TFSA]) and oligoethers (tetraglyme (G_4), triglyme (G_3), diglyme (G_2), and monoglyme (G_1)) or tetrahydrofuran (THF). As shown in Fig. 7a, the peak shifted to a higher frequency in the sequence $[Li(THF)_4] < [Li(G_3)_1] < [Li(G_2)_{4/3}] < [Li(G_1)_2]$. The solvate ILs $[Li(G_3)_1][TFSA]$ and $[Li(G_2)_{4/3}][TFSA]$ significantly suppressed oxidative decomposition, contrary to notable decomposition observed in concentrated $[Li(THF)_4]$–[TFSA] and $[Li(G_1)_2][TFSA]$ solutions at lower potentials.[72]

As shown in Fig. 8, the discharge capacities of cells with $[Li(THF)_4][TFSA]$ and $[Li(G_1)_2][TFSA]$ are higher than those of cells with $[Li(G_2)_{4/3}][TFSA]$ and $[Li(G_3)_1][TFSA]$. The reason is related to the differences in viscosity and ionic conductivity of the electrolytes. The viscosities and ionic conductivities of $[Li(THF)_4][TFSA]$ and $[Li(G1)_2][TFSA]$ are low and high, respectively, in comparison with those of $[Li(G_2)_{4/3}][TFSA]$ and $[Li(G_3)_1][TFSA]$. In both $[Li(THF)_4][TFSA]$ and $[Li(G_1)_2][TFSA]$ electrolytes, the solubility of lithium polysulfides was rather high.[73]

A newly designed ionic liquid (RTIL)-electrolyte has been suggested to create a trade-off between the solubility and diffusion rate of lithium polysulfides by mixing the high lithium polysulfide solubility of 1,2-dimethoxyethane (DME) and the high viscosity of *N*-methyl-*N*-propyl piperidinium bis(trifluoromethanesulfonyl)imide (PP13-TFSI). As shown in Fig. 9, the discharge capacity values at 0.1 C were 1360 and 1300 mA h g^{-1} for the first and second cycles, which was more than twice that with the 100% DME electrolyte.[74]

In another study, the effects of different IL electrolytes were investigated and it was proved that 1-butyl-1-C4mpyr-TFSI (methyl pyrrolidinium bis(trifluoromethanesulfonyl)imide) could be a promising candidate as a Li–S battery electrolyte with a coulombic efficiency of greater than 99% over 100 cycles. With a high conductivity and low viscosity, C4mpyr-TFSI could enhance the battery performance.[75] In summary, ILs with high conductivity, high coulombic efficiency, improved capacity retention, and restrained shuttle effect are promising electrolytes for high-rate Li–S batteries.[76–79]

4. Solid electrolytes (SEs)

Solid electrolytes are essential components for high-performance Li–S batteries. Batteries with SEs provide better safety, a higher energy density, a longer life cycle and a suppressed shuttle effect.[80–84] Currently, two main types of SEs are investigated in

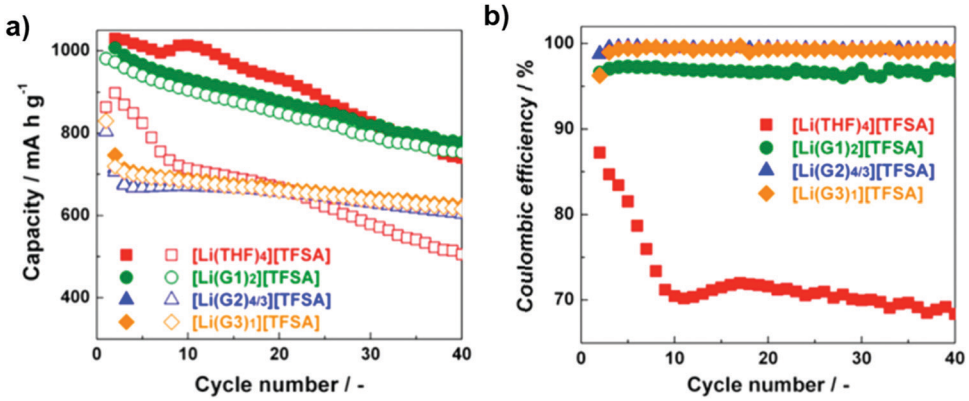

Fig. 8 Cycling performance of Li–S cells with [Li(glyme or THF)$_x$][TFSA] (a) capacity; and (b) coulombic efficiency. Image reprinted with the permission from ref. 73. Copyright © 2015, Elsevier License 5041351036896.

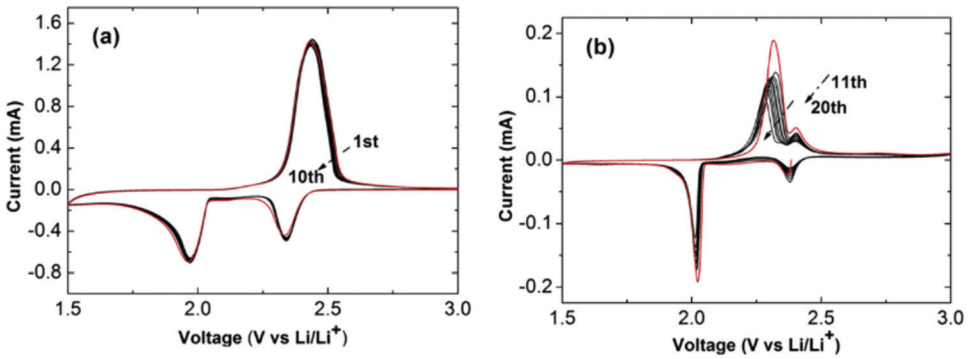

Fig. 9 CV curves of Li–S cells with 1 M LiTFSI in PP13-TFSI/DME (2/1, v/v). (a) The first 10 cycles at 0.1 mV s^{-1} and (b) the subsequent 10 cycles. Image reprinted with the permission from ref. 74. Copyright © 2013, Elsevier License 5041360562040.

which one type is solid polymer electrolytes such as poly(ethylene oxide), poly(acrylonitrile), poly(vinylidene fluoride), and poly-(phenylene oxide)[85–90] and the other type is inorganic solid electrolytes, in particular sulfides and oxides including Li_2S–P_2S_5, Li_6PS_5X (X = Cl, Br, I), $Li_7La_3Zr_2O_{12}$, and Ti/Ge-based lithium phosphate and perovskites.[91–99]

4.1 Polymer electrolytes

Polymer electrolytes can be classified into solid polymer electrolytes (SPEs) and gel polymer electrolytes (GPEs). SPEs have advantages such as a high mechanical stability, the formation of a stable interface with Li metal, and the inhibition of Li dendrite formation. To alleviate the polysulfide shuttle effect, an electrolyte containing $PEO_{18}Li(CF_3SO_2)_2N$–10 wt% SiO_2 was suggested to replace the common organic electrolyte, which functions to suppress polysulfides. A cell with the $PEO_{18}Li(CF_3SO_2)_2N$–10 wt% SiO_2 electrolyte and a cathode containing 60 wt% of the as-prepared sulfur in ordered mesoporous carbon spheres (S–OMCs) composite, 20 wt% PEO binder and 20 wt% acetylene black was assembled in an argon-filled glove box. As shown in Fig. 10, the S–OMCs composite exhibits excellent cycling stability with a discharge capacity of 800 mA h g^{-1} after 25 cycles and the capacity retention of 65%. Also, the sulfur on the lithium anode was low, meaning that this novel cell can readily provide a good electrical path for the sulfur products during cycling.[100]

Nanostructured block copolymer electrolytes, including polystyrene-*b*-poly(ethylene oxide) (SEO) doped with lithium bis(trifluoromethanesulfonyl)imide (LiTFSI), were investigated as a high-ionic-conductivity electrolyte to prevent dendrite formation. Additionally, it shows a stable interface with the lithium metal anode.[101,102] The phase behavior of SEO/Li_2S_x mixtures could be better than mixtures of SEO and other lithium salts. The thermal properties of the SEO copolymers with Li_2S_x were investigated in Fig. 11a at a constant concentration of r = 0.085. The melting temperature, T_m, and the enthalpy of melting, ΔH_m, of the crystalline structures decrease with increasing polysulfide length. The UV-vis spectra from the SEO (1.7–1.4)/Li_2S_x was performed to observe interactions between the salt and the PEO block. The qualitative similarity of the spectra of all of the samples in Fig. 11b indicates that all of the samples include similar species. A dominant peak at 480 nm in all samples is the most prominent peak in SEO (1.7–1.4)/Li_2S_2, confirming the presence of the S_2^{2-} anion in all samples.[103]

Gel polymer electrolytes demonstrate several advantages, including a higher conductivity than solid polymer electrolytes

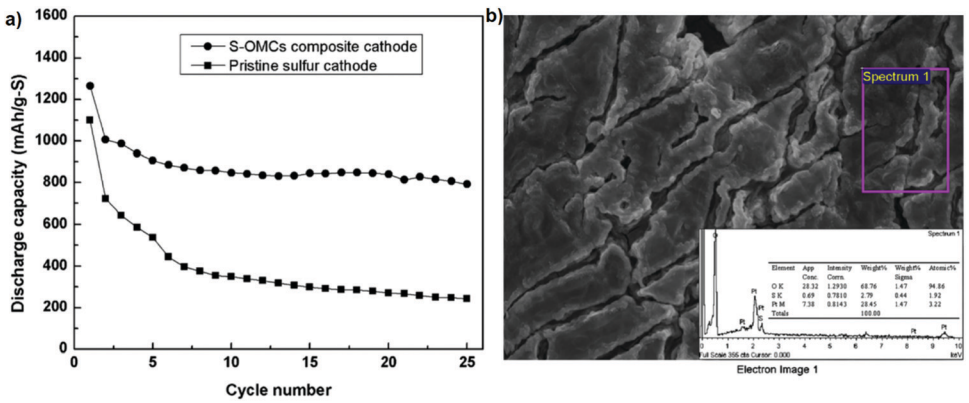

Fig. 10 (a) Cycling performance of the Li/S half-cell. (b) EDS spectrum of the surface of the lithium anode with the S–OMCs composite. Image reprinted with the permission from ref. 100. Copyright © 2011, Elsevier License 5041371180906.

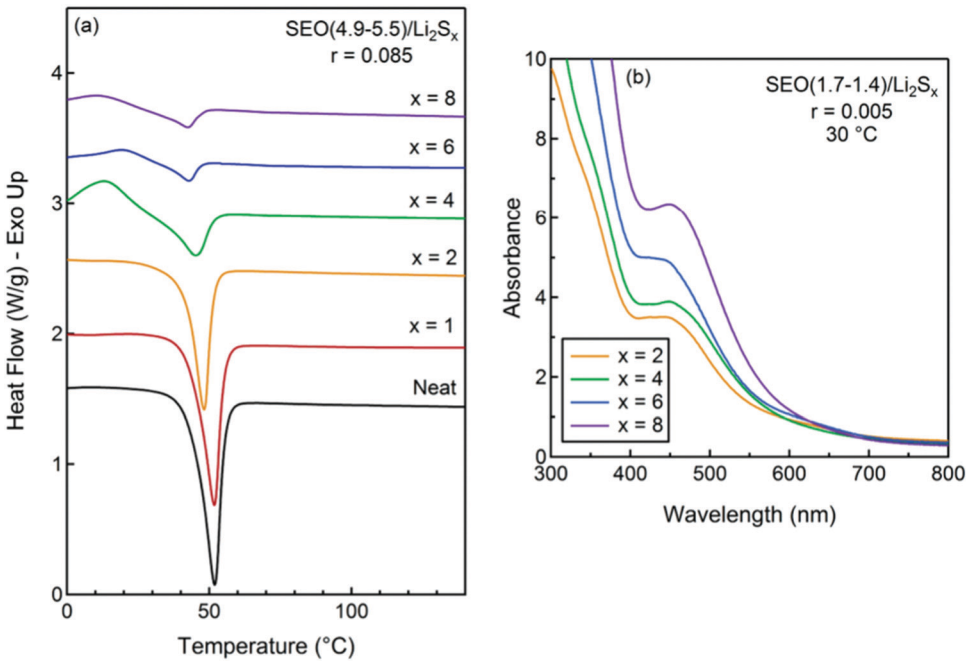

Fig. 11 (a) DSC traces of SEO (4.9–5.5)/Li_2S_x at r = 0.085 and a heating rate of 10 °C min^{-1}, and (b) UV-vis spectra of dry mixtures of Li_2S_x at r = 0.005 in SEO (1.7–1.4) at 30 °C. Image reprinted with the permission from ref. 103. Copyright © 2011, American Chemical Society.

and mechanically stable properties. They have been investigated recently to overcome the capacity-fading issue. A gel polymer electrolyte (GPE) prepared by combining a porous membrane with the *N*-methyl-*N*-butylpyrrolidinium bis(trifluoromethanesulfonyl)imide ionic liquid exhibits an acceptable thermal stability and high anodic oxidation capability. The Li/S battery with the GPE electrolyte delivers a low initial discharge capacity of 1217.7 mA h g^{-1}, indicating incomplete conversion of the first-cycle discharge product. As the number of cycles increases, the cell exhibits good capacity retention, which may be due to the reduced solubility of the polysulfides in the GPE electrolyte, which subsequently reutilizes the active sulfur during the cycling process[104] (Fig. 12a and b). Fig. 12c and d depicts the non-Arrhenius VTF action of the GPE's ionic conductivity as a function of temperature. At room temperature, the GPE had an ionic conductivity of 2.54×10^{-4} S cm^{-1}, which was comparable to the GEP with a mesoporous SiO_2 filler prepared by solution casting.

A free-standing gel polymer electrolyte was prepared by soaking the membrane in 1 M $LiPF_6$ dissolved in a 1 : 1 (v/v) mixture of ethylene carbonate (EC) and diethylene carbonate (DEC) for 30 min. The acronym mGPE was considered for the as-prepared modified gel polymer electrolyte. The Li/mGPE/S cell delivers a superior capacity retention of 1050 mA h g^{-1} after 100 cycles, about 88% of the initial value. The unique porous configuration of the membrane contributes to the capacity enhancement, which maintains the electrolyte solution and suppresses the dissolution of polysulfides[105] (Fig. 13).

The composite gel polymer electrolyte (CGPE) with a 50PEO–50SiO_2 (wt%) composite-coated separator (C-separator) has been suggested by Zhang *et al.* to improve the safety and performance of the Li–S battery. The cell polarization remains constant when cycling at a high current density, indicating that the discharge and charge voltage profiles are identical. The rate capability of the Li/S cells with a C-separator and CGPE is evaluated in Fig. 14b. The capacity declined much faster at low current densities. By increasing current densities and cycle numbers, the capacity held stable at 550–560 mA h g^{-1} at the end of the test.[106]

Fig. 14c shows the wettability of the liquid electrolyte on the P-separator and C-separator after a 5 μL liquid electrolyte droplet was dropped onto the separator from a height of about 1 cm. The liquid electrolyte seemed to have a lower touch angle and spread further on the C-separator than on the P-separator. To show the stickiness of the shaped CGPE, a few droplets of liquid electrolyte were added to the C-separator, and the wetted separator was instantly used to glue a stainless-steel cup, discovering that the wetted C-separator could easily pick the cup up from the desk (Fig. 14d). This progress is due to the composite coating's highly porous nature and its high SiO_2 content.

Poly(vinylidene fluoride-*co*-hexafluoropropylene)/poly(methyl methacrylate)/silicon dioxide (PVDF-HFP/PMMA/SiO_2) was investigated as a GPE by Bakenov *et al.* The GPE battery delivered discharge capacities of 809 and 413 mA h g^{-1} at the 1st and 50th cycles at 0.2 C, respectively. An impedance plot for the PVDF-HFP/PMMA/SiO_2 composite electrode demonstrates no semicircles, implying that the total conductivity of the polymer electrolyte originated mainly from the ionic conduction. The GPE membrane delivered a high room-temperature ionic conductivity of 3.12 mS cm^{-1}. The CV data of the GPE had no breakdown during cycling, proving that the GPE is electrochemically stable over the operation range of the Li/S cell[107] (Fig. 15).

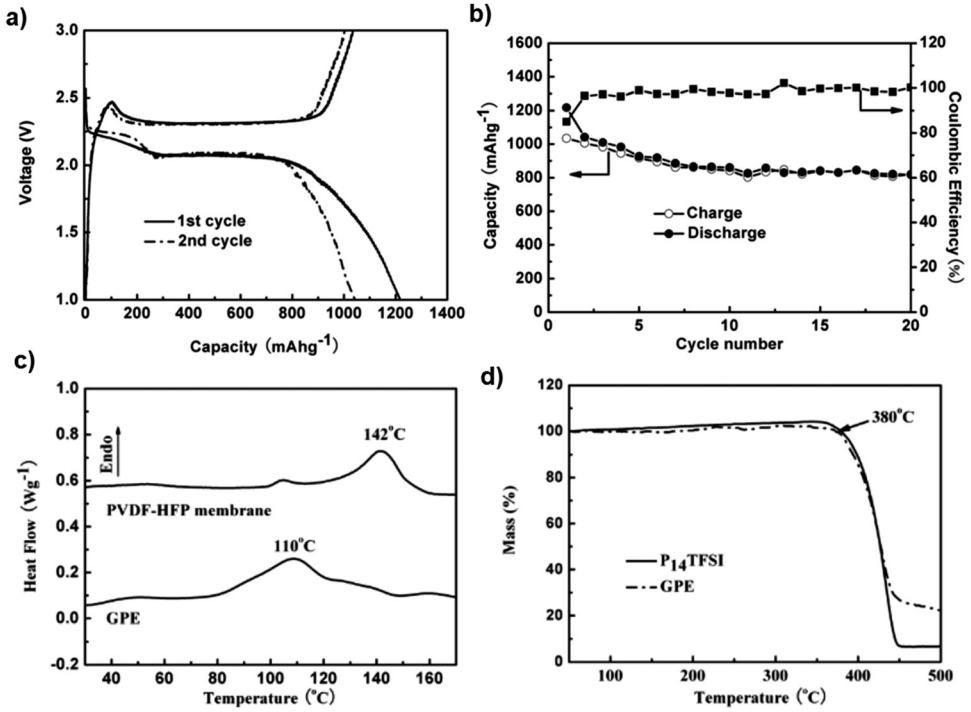

Fig. 12 (a) Charge–discharge curves and (b) cycling performance of the Li/GPE/S battery at a current density of 50 mA g^{-1}. (c) DSC curves of P(VDF-HFP) membrane and GPE, and (d) TGA of P_{14}TFSI and GPE. Image reprinted with the permission from ref. 104. Copyright © 2012 Elsevier License 5041380226718.

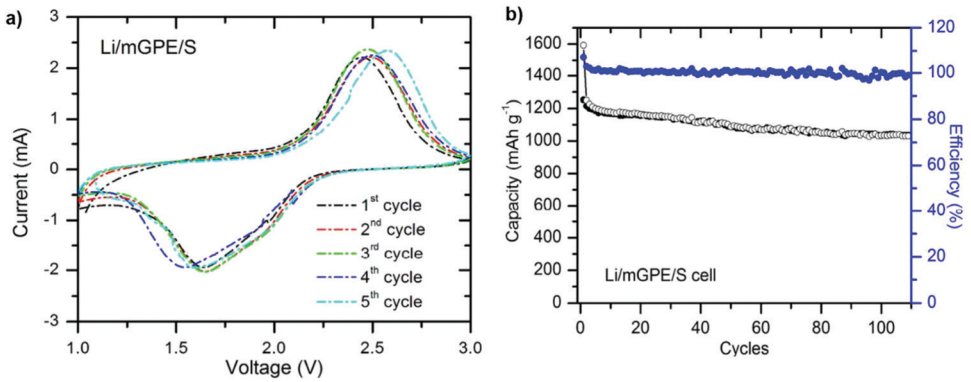

Fig. 13 (a) CV profiles for the Li/mGPE/S cell and (b) charge–discharge *versus* cycles at a 0.2 C rate. Image reprinted with the permission from ref. 105. Copyright © 2013, Royal Society of Chemistry License 1116861-1.

The double-layer gel polymer electrolyte is an interesting idea, which includes the transition layer composed of polyacrylonitrile (PAN), polyethylene oxide (PEO) and $Li_{1.3}Al_{0.3}Ti_{1.7}(PO_4)_3$ (LATP) on the Li anode side to alleviate the passivation effect. Additionally, LATP with a higher ionic conductivity can act as the Li^+ transport channel to further enhance the ionic conductivity of the composite membrane. The pure PAN electrolyte membrane has a T_g of 90.1 °C. After adding PEO, the T_g of the PAN decreases to 86.0 °C. The intermolecular hydrogen-bonding effect between PAN and PEO enables polymer chains to be more chaotic, which increases the amorphous regions. The endothermic peak of the PAN + PEO electrolyte membrane further declines to low temperature after adding LATP, indicating that the addition of LATP can reduce the crystallinity[108] (Fig. 16).

In summary, a GPE could function as an efficient electrolyte material for Li–S batteries with high flexibility and volume toleration as well as good compatibility with the electrodes.[109–111]

4.2 Inorganic solid electrolytes

Various inorganic electrolytes such as Li_2S–SiS_2, $Li_{1.5}Al_{0.5}Ge_{1.5}(PO_4)_3$ (LAGP), Li_3PS_4, thio-LISICON $Li_{3.25}Ge_{0.25}P_{0.75}S_4$, $Li_{10}MeP_2S_{12}$ (M = Ge, Sn, Si), $Li_{9.54}Si_{1.74}P_{1.44}S_{11.7}C_{l0.3}$, and Li_6PS_5X (X = Cl, Br, I) and oxides (*e.g.*, garnet-type $Li_7La_3Zr_2O_{12}$, NASICON-type Ti/Ge-based lithium phosphate, and perovskites) have been developed as solid electrolytes in all-solid-state Li–S batteries.[112–129]

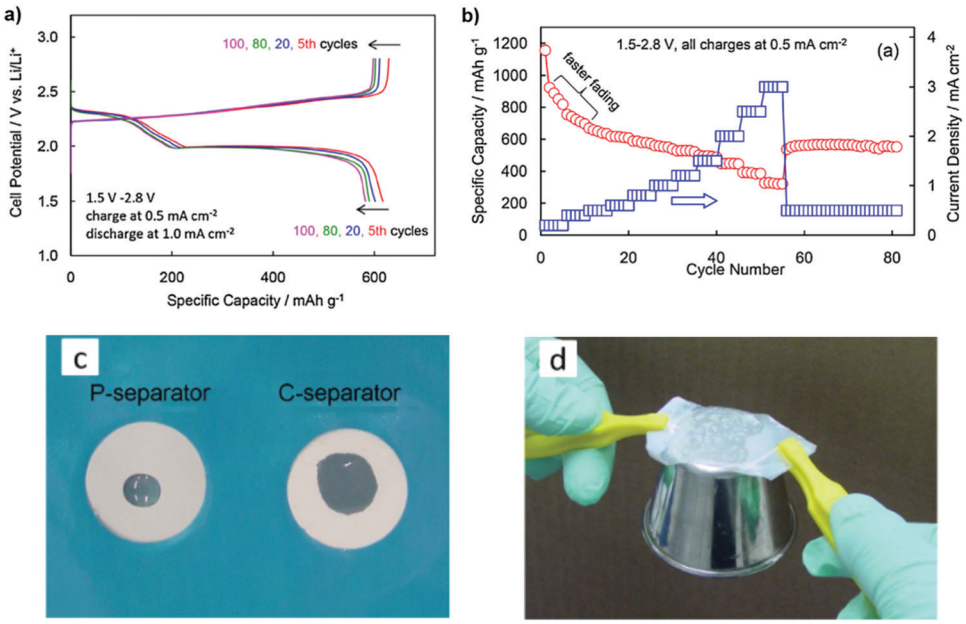

Fig. 14 (a) Voltage profile in selected cycles and (b) rate capability of the Li/S cell with the C-separator. (c) Wettability of the liquid electrolyte on separator and (d) gluing ability of the C-separator immediately after being wetted with a liquid electrolyte. Image reprinted with the permission from ref. 106. Copyright © 2013, Elsevier License 5041390032620.

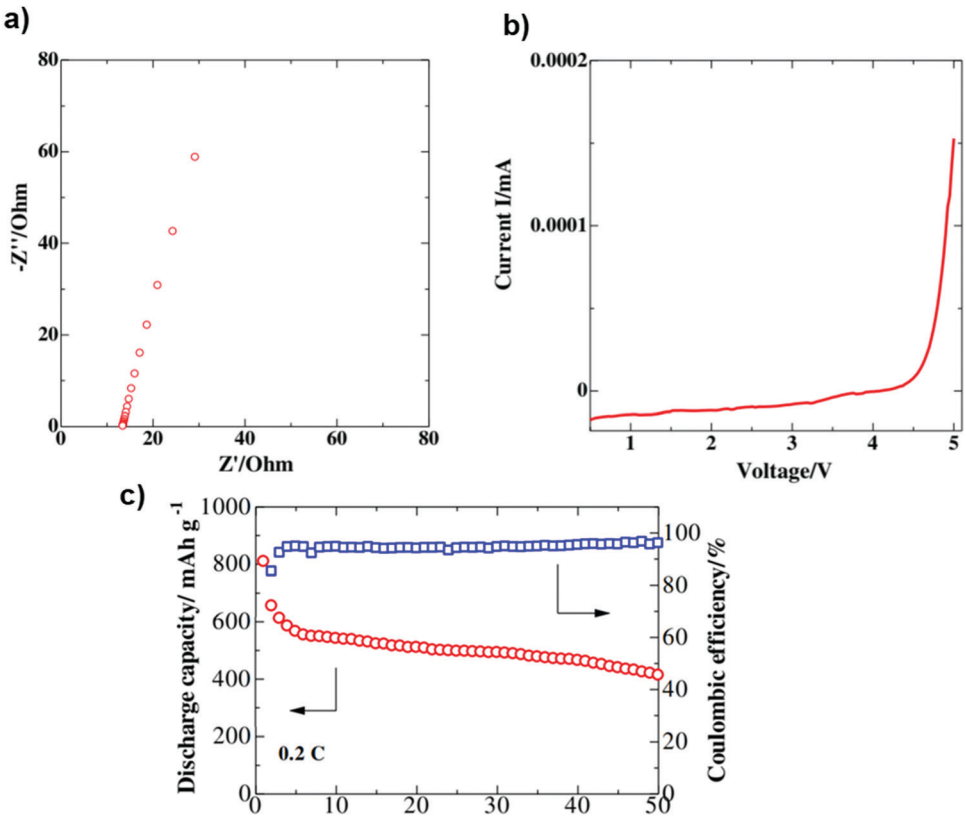

Fig. 15 (a) Impedance spectrum of the as-prepared gel polymer electrolyte. (b) CV profile of the Li/GPE/SS cell (scan rate 0.1 mV s^{-1}). (c) Cycling performance of the gel polymer cell with S/GNS composite cathode at 0.2 C. Image reprinted with the permission from ref. 107. https://doi.org/10.1186/1556-276X-9-137.

Li_2S–GeS_2–P_2S_5 thio-LISICON has superior ionic conductivity, but its low compatibility with lithium metal and the high cost of germanium have limited its practical applications. Other sulfides, such as SnS_2 and SiS_2, have been considered to substitute GeS_2

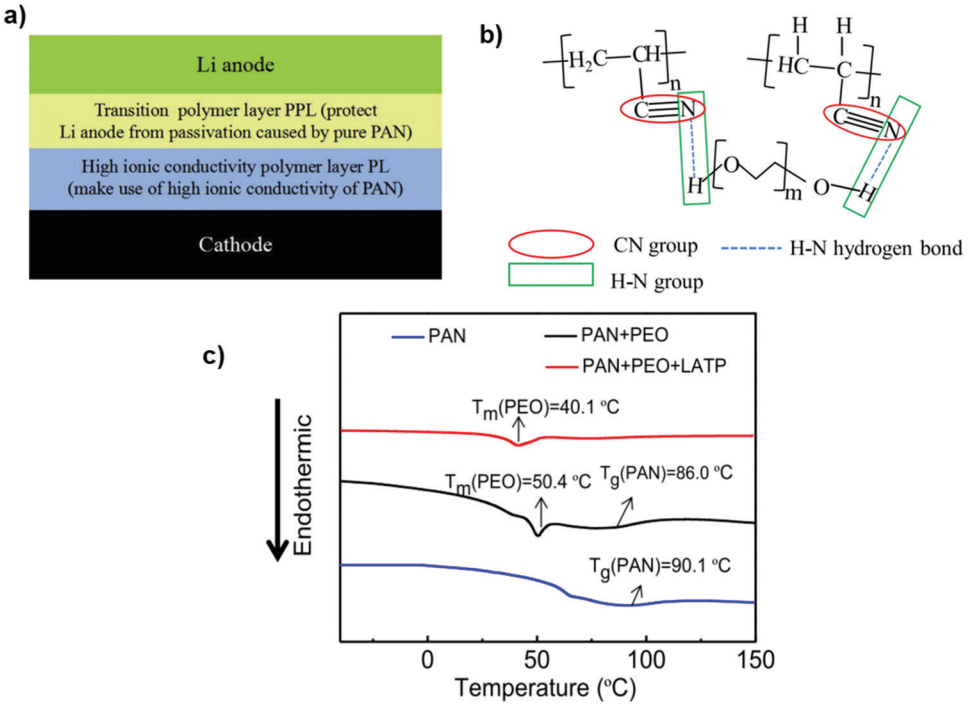

Fig. 16 (a) Working mechanism and stacking model of the PPL-PL electrolyte. (b) Schematic diagram of the intermolecular hydrogen-bonding effect between PAN and PEO and the passivation-weakening mechanism of CN groups by hydrogen bonds. (c) DSC curves of PAN, PAN + PEO, and PAN + PEO + LATP. Image reprinted with the permission from ref. 108. Copyright © 2019, Elsevier License 5041391264234.

and to provide superionic conductor materials.[130] The application of an electrolyte using a $Li_{1.5}PS_{3.3}$ {$60Li_2Se_{40}P_2S_5$ (mol%)} was investigated recently and showed a capacity of 1096 mA h g^{-1} under 6.4 mA cm^{-2}. As shown in Fig. 17, the cycling performance of the all-solid-state Li/S cell with $Li_{1.5}PS_{3.3}$ and $Li_{4.0}PS_{4.5}$ were investigated. The coulombic efficiency was approximately 100% over 50 cycles. The cell with the $Li_{1.5}PS_{3.3}$ electrolyte displayed an excellent cycling performance. The capacity of the cell is greater than 1200 mA h g^{-1} for 50 cycles.[131]

One of the optimized configurations for the Li–S cell is classified as Li_2S–P_2S_5 as the glass-type electrolyte, with lithium metal as the anode and a graphite–sulfur compound as the cathode material. The high-capacity retention of 400 mA h g^{-1} at a working voltage of 2.1 V for the glass-type electrolyte is higher than that with the common organic carbonate electrolytes, which are characterized by a capacity of 150 mA h g^{-1} at a working voltage of 3.6 V[132] (Fig. 18).

By developing a solid-state Li–S battery using $0.75Li_2S$–$0.25P_2S_5$, with Li_3PS_4 as the electrolyte, the battery delivered a capacity of 1600 mA h g^{-1} with a satisfactory capacity retention. The XRD pattern showed no peaks matching Li_2S and P_2S_5, implying the formation of Li_3PS_4. Nyquist plots of the

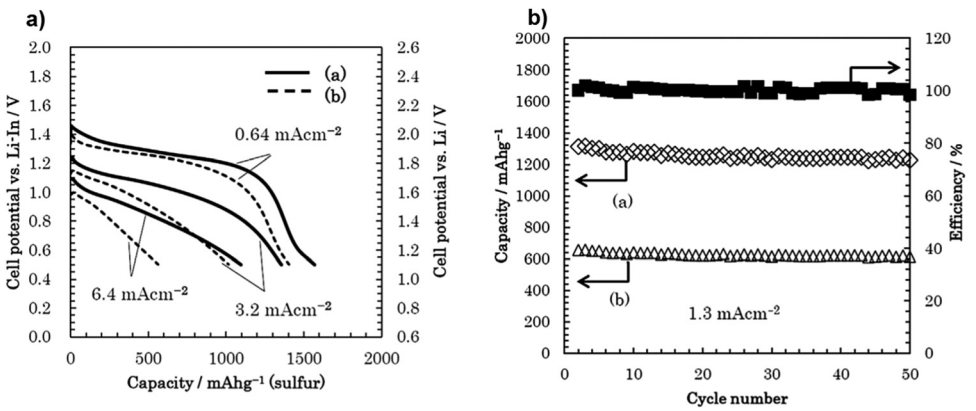

Fig. 17 (a) Discharge curves of the all-solid-state Li/S cells with positive composite electrodes using (a) $Li_{1.5}PS_{3.3}$ and (b) $Li_{4.0}PS_{4.5}$. (b) Cycling performance of an all-solid-state Li/S cell with a positive composite electrode using $Li_{1.5}PS_{3.3}$ and $Li_{4.0}PS_{4.5}$ under 1.3 mA cm^{-2}. Image reprinted with the permission from ref. 131. Copyright © 2019, Elsevier License 5041391484159.

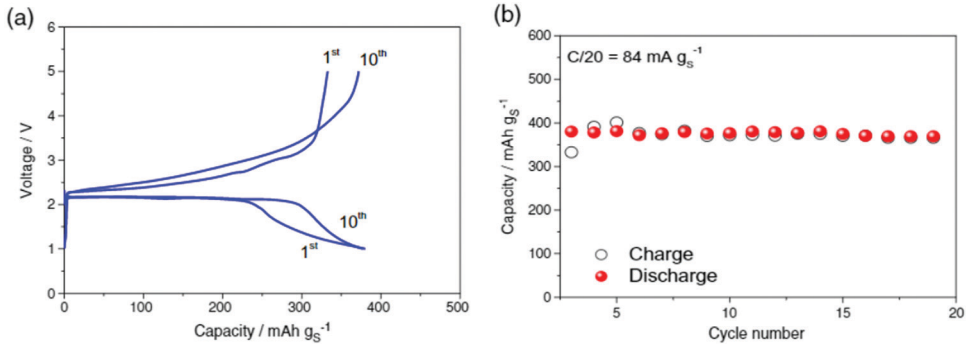

Fig. 18 (a) Voltage profiles and (b) cycling behavior of a Li/Li_2S–P_2S_5/S–MCMB cell. Image reprinted with the permission from ref. 132. Copyright © 2021, Elsevier License 5041400972622.

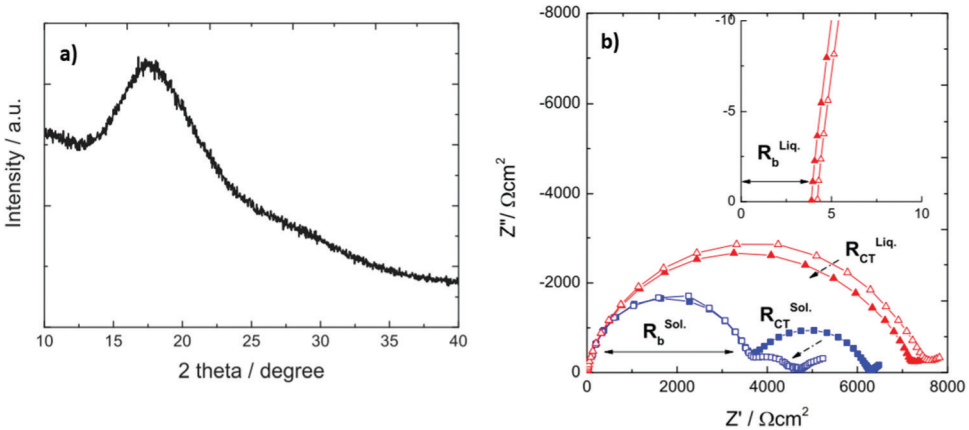

Fig. 19 (a) XRD diffraction pattern of Li_3PS_4 and (b) Nyquist plots of solid (blue) and liquid (red) electrolyte symmetrical Li/Li cells at −20 °C. Image reprinted with the permission from ref. 133. Copyright © 2015 IOP publishing *J. Electrochem. Soc.* https://doi.org/10.1149/2.0441504jes.

solid- and liquid-electrolyte cells at −20 °C are shown in Fig. 19b. The solid electrolyte cell (blue squares) displays a different frequency response. At −20 °C, the R_{CT} of the liquid electrolyte cell is much larger than that of the solid electrolyte cell, demonstrating that the solid electrolyte is very effective in physically preventing polysulfide migration.[133]

All-solid-state batteries with Li_6PS_5Br as the electrolyte have been suggested using the argyrodite electrolyte for a high-performance all-solid-state Li–S battery. Adams *et al.* reported the cell with Li_6PS_5Br as the solid electrolyte, with a discharge capacity of 1460 mA h g^{-1}. After 50 cycles at the rate of C/10, a cell with 20% S delivered an initial discharge capacity of 1355 mA h g^{-1} and capacity retention of 1080 mA h g^{-1}. It demonstrates that in the second cycle, the discharge capacity decreases to 1150 mA h g^{-1}, due to the severe volume change of the active material during cycling. During cycles 2–50, the discharge capacity delivered an average fading of 0.13% per cycle, implying a high-capacity retention of 94% for 49 cycles, with a reversible capacity of 1080 mA h g^{-1} at the 50th cycle. The Columbic efficiency had an average value of 100% over cycles 2–50, suggesting the efficient reutilization of the active material[134] (Fig. 20).

To improve the effect of the inorganic solid electrolyte, the interface stability between the $Li_{10}GeP_2S_{12}$ (LGPS) solid electrolyte and Li metal was modified by employing an ionic liquid such as 1 M lithium bis-(trifluoromethanesulfonyl)imide (LiTFSI)/*N*-methyl-*N*-propylpyrrolidinium bis(trifluoromethanesulfonyl) imide (PYR13TFSI) as the interface modifier. The result demonstrated high sulfur utilization and also an enhancement of the intimate contact between the electrode and the LGPS solid electrolyte during the cycling. It can be observed from Fig. 21 that the Li/LGPS/Li cells modified with 1 M IL showed a flat and highly stable profile with a small over-potential, even after a prolonged 1200 h, emphasizing a remarkable improvement in the cycling stability. SEM images on the LGPS surface after long-term stripping/plating cycles proved that the 1 M IL can efficiently protect against unfavorable side reactions between the LGPS and Li metal, resulting in the smooth surface morphology observed. However, LGPS without the IL showed significant voids from unfavorable reactions with the Li metal, leading to a black color.[135]

5. Novel hybrid electrolytes

The low cycle efficiency and lithium dendrite formation during cycling are the most important challenges which hinder the practical application of the Li–S cell. A new dual-salt electrolyte composed of $Li[N(SO_2F)_2]$ and $Li[N(SO_2CF_3)_2]$ has been

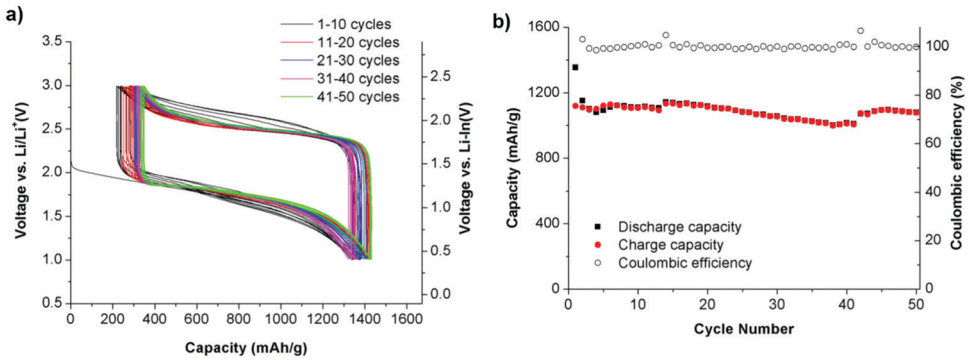

Fig. 20 (a) Discharge–charge curves and (b) discharge/charge capacity and coulombic efficiency of the all-solid-state S/Li_6PS_5Br/In–Li cell up to 50 cycles at room temperature. Image reprinted with permission from ref. 134. https://doi.org/10.1007/s10008-014-2654-1.

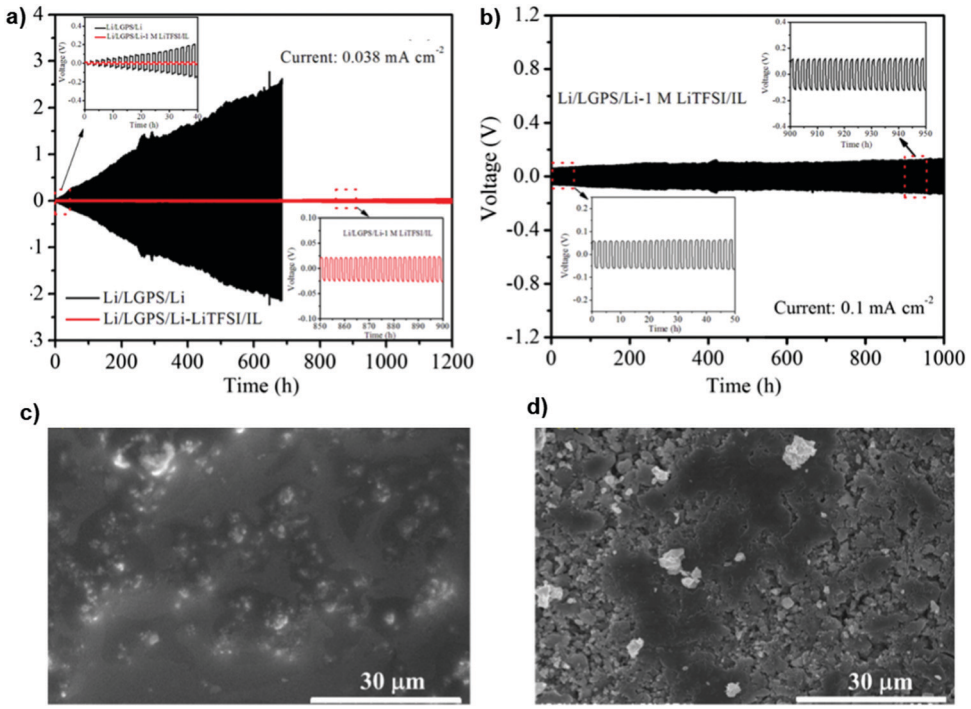

Fig. 21 (a) Galvanostatic cycling curves of cells with and without 1 M LiTFSI/IL at 0.038 mA cm^{-2} and (b) the cell with 1 M LiTFSI/IL. SEM images after long-term Li stripping/platting cycles for the cells (c) with and (d) without 1 M LiTFSI/IL. Image reprinted with permission from ref. 135. Copyright © 2019, American Chemical Society.

suggested to overcome these two problems. The formation of a unique protection film in the electrolyte solution could improve the Li crystal growth pattern with the dendrite-free surface of the anode. Additionally, the high cycling performance and unique lithium morphology can be achieved even at a high current density of 10 mA cm^{-2}. As shown in Fig. 22a, deposition of Li on the anode surface using the dual-salt electrolyte was tidy with a dense particle array, implying a suitable site for forming a high-quality SEI layer. Moreover, Fig. 22b showed no lithium dendrite formation after 51 cycles at a high current density of 10 mA cm^{-2}.[136]

N-Methoxyethyl-*N*-methyl pyrrolidinium bis(trifluoromethanesulfonyl)imide ($Pyr_{1,2O1}TFSI$) and tri(ethylene glycol)dimethyl ether (TEGDME) in a mass ratio of 7 : 3 were investigated recently as a novel electrolyte to support the Li–S cell with a high cycling stability. Moreover, lithium difluoro(oxalate) borate (LiODFB) was added to enhance the viscosity of the electrolyte. Fig. 23b shows the CV curves with a scan rate of 0.1 mV s^{-1} for the Li–S cells with the $Pyr_{1,2O1}TFSI$/TEGDME electrolyte with LiTFSI or LiODFB as the lithium salts. The two reduction peaks in the CV curve of the cell with LiTFSI corresponded to the formation of long-chain polysulfides at 2.2–2.4 V and then conversion to short-chain lithium polysulfides below 2.0 V. However, the CV curve of the cell with LiODFB demonstrates reduction/oxidation peaks with a small area, indicating the weak redox reactions.[137]

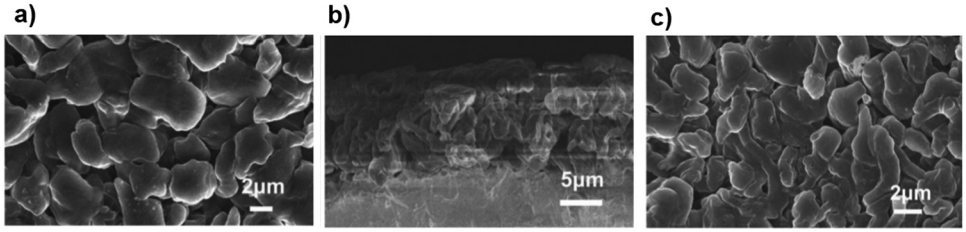

Fig. 22 (a) SEM micrographs of a Li electrode after 10 cycles at 2 mA cm^{-2} in LiFSI–LiTFSI/DOL–DME electrolyte. (b) Cross-section micrograph of metallic lithium after 5 cycles in the LiFSI–LiTFSI/DOL–DME electrolyte. (c) SEM micrograph of lithium deposited after 51 cycles in LiFSI–LiTFSI/DOL–DME solution at 10 mA cm^{-2}. Image reprinted with permission from ref. 136. Copyright © 2020, Royal Society of Chemistry License 1116857-1.

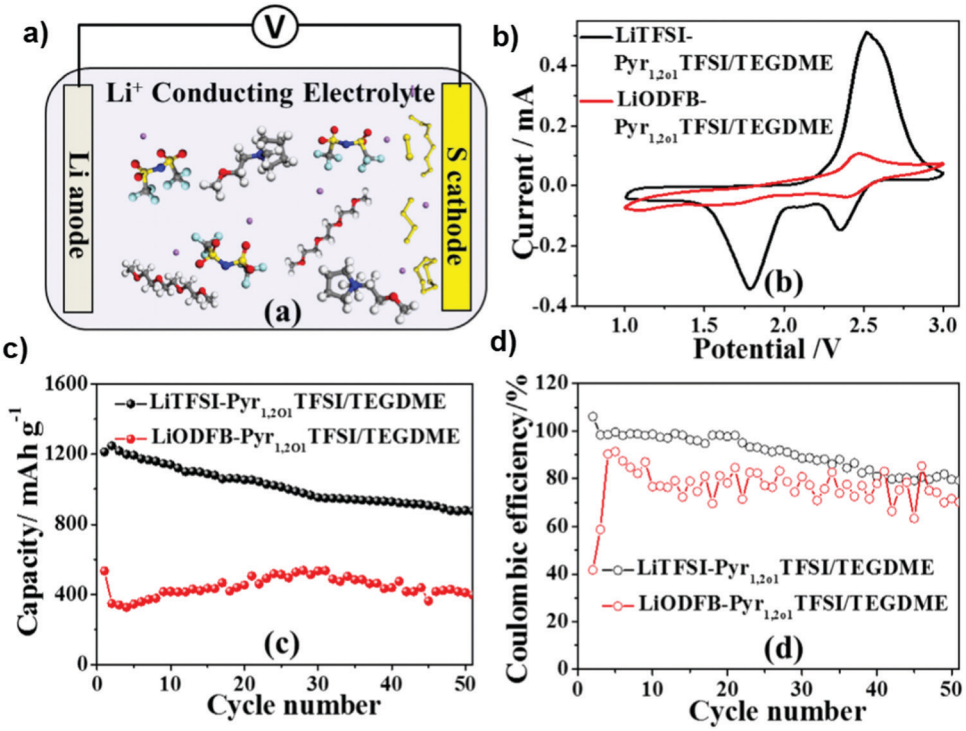

Fig. 23 (a) Schematic illustration of the $Pyr_{1,2O1}$TFSI/TEGDME electrolyte with LiTFSI. (b) CVs of the Li–S cells containing the $Pyr_{1,2O1}$TFSI/TEGDME electrolytes with LiTFSI and LiODFB. (c) Cycling performance and (d) coulombic efficiency of the Li–S cells with the LiTFSI-$Pyr_{1,2O1}$TFSI/TEGDME and LiODFB-$Pyr_{1,2O1}$TFSI/TEGDME electrolytes. Image reprinted with permission from ref. 137. Copyright © 2015, Elsevier License 5041420221520.

Fig. 23c and d show the cycling performance and coulombic efficiency of Li–S cells containing the electrolyte with LiTFSI or LiODFB at 0.1 C. The initial discharge capacity of the Li–S cell containing LiTFSI-$Pyr_{1,2O1}$TFSI/TEGDME was 1212.8 mA h g^{-1} and retained a value of 896 mA h g^{-1} after 50 cycles. The cell with the LiODFB-$Pyr_{1,2O1}$TFSI/TEGDME electrolyte exhibited severe capacity fading due to the formation of an excessive passivation film, which hindered the electrochemical reduction of the polysulfides.[137] In a recent study, composite electrolyte membranes consisting of the polyacrylonitrile (PAN)–$Li_{6.5}La_3Zr_{1.5}Ta_{0.5}O_{12}$ (LLZTO) matrix as well as $LiClO_4$ and $Mg(ClO_4)_2$ dual salts were prepared by electrospinning. It was found that the cycle stability of the lithium metal battery was improved by adding the magnesium salt to the electrolyte membrane. Fig. 24a shows the long-term cycling performance of the cells with different electrolytes at the 0.5 C rate. The battery with an electrolyte without magnesium salt shows a capacity of 137 mA h g^{-1} after 100 cycles, with a capacity retention of 93%. The capacity of the cell quickly declines to 50 mA h g^{-1}, with a capacity retention of 34%. For the cell with the magnesium-salt-containing electrolyte, the capacity of the battery can be retained at 150 mA h g^{-1} and there is no fading for 300 cycles. The cells were disassembled after testing for 200 cycles. The surface of the lithium metal electrode was investigated by SEM. SEM images of the surface of the metal lithium electrode of the cell with the magnesium-salt-containing electrolyte show that it is relatively smooth with small cracks on the surface of the lithium foil. It is found that the addition of magnesium salt can effectively protect the lithium metal anode, alleviate cracking and hinder the growth of lithium dendrites.[138] Thus, the dual-salt electrolyte also formed a very thin and dense inorganic layer that functions as a protective layer to suppress Li dendrite

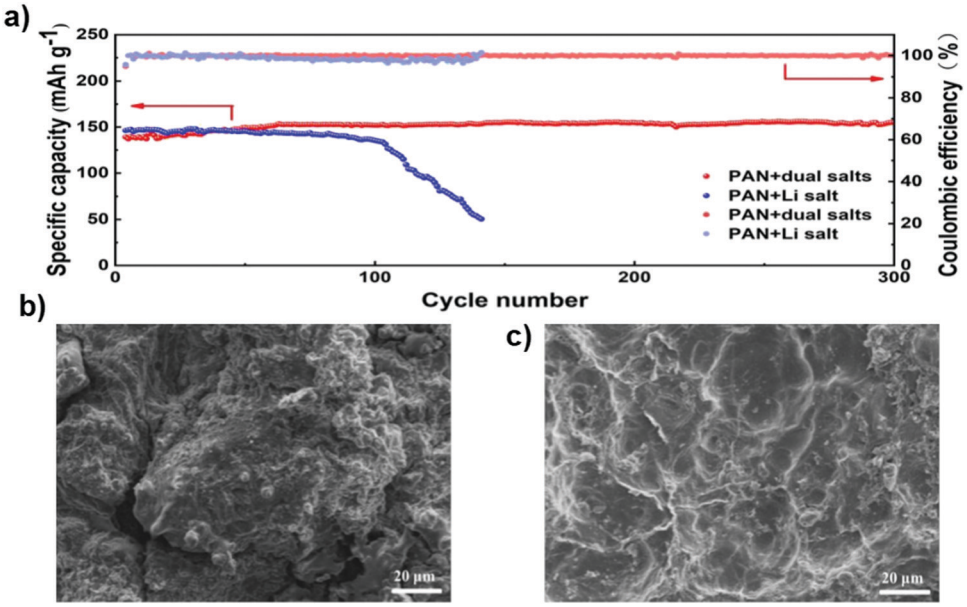

Fig. 24 (a) Long-term cycling performance of cells with different electrolytes at the 0.5 C rate. (b) SEM image of the surface of the metal lithium electrode in cells, without the magnesium salt added to the electrolyte, after 200 cycles, and (c) SEM image of the surface of the metal lithium electrode in the cells, with magnesium salt added to the electrolyte, after 200 cycles. Image reprinted with permission from ref. 138. Copyright © 2020, Royal Society of Chemistry License 1116857-1.

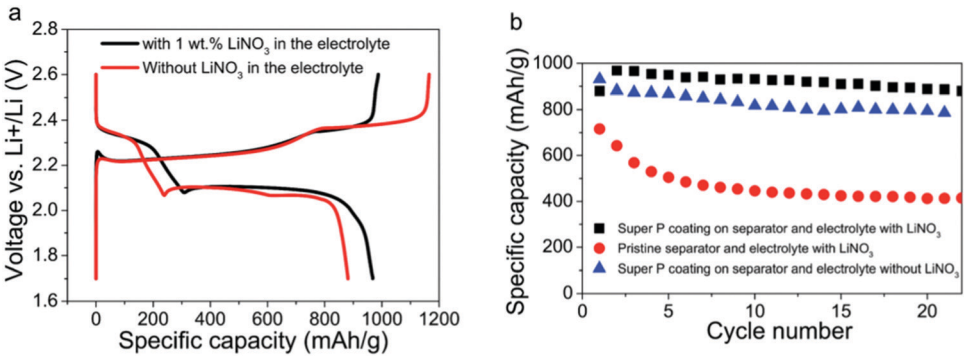

Fig. 25 (a) First charge/discharge voltage profiles of the Li–S batteries using the electrolyte with and without 1 wt% $LiNO_3$, respectively. (b) Cycling stability comparison of the Li–S batteries with different separators and electrolytes at C/10. Image reprinted with the permission from ref. 139. Copyright © 2014, Royal Society of Chemistry License 1116742-1.

formation, resulting in the facial deposition of uniform lithium grains.

6. Electrolyte additives

The discovery of additives in liquid electrolytes was an innovation for Li protection in Li/S batteries. It has been reported that $LiNO_3$ contributes to the formation of a stable passivation film, also known as a "solid electrolyte interface (SEI)," on the surface of a Li anode. In a recent study, a freshly prepared solution of LiTFSI (1 M) in 1 : 1 v/v DME and DOL containing lithium nitrate ($LiNO_3$ (1 wt%)) was tested with a conductive coating on the separator. This surface-modified separator and ether electrolyte with and without $LiNO_3$ were investigated, and the specific capacity and cycling stability of the Li–S batteries was improved compared with the batteries that had pristine separators. An initial specific capacity of 1350 mA h g^{-1} at C/2 and a decay rate as low as 0.09% per cycle over 500 cycles[139] was demonstrated (Fig. 25).

1 M LiTFSI and 0.5 M $LiNO_3$, in a solvent mixture of DOL and DME (1 : 1), was considered as an efficient electrolyte for polysulfide trapping. The boron (B) dopant with positive polarization in the TiO_2 structure is inserted as an interlayer on a glass fiber separator. The B-doped (at 1% and 5%) TiO_2-coated separators with the as-prepared electrolyte delivered higher capacities of 1001 and 1293 mA h g^{-1}, respectively, after 100 cycles at 1 C after 100 cycles[140] (Fig. 26).

The addition of $LiNO_3$ could contribute to the electrode–electrolyte interface modification and provide a stable passivation

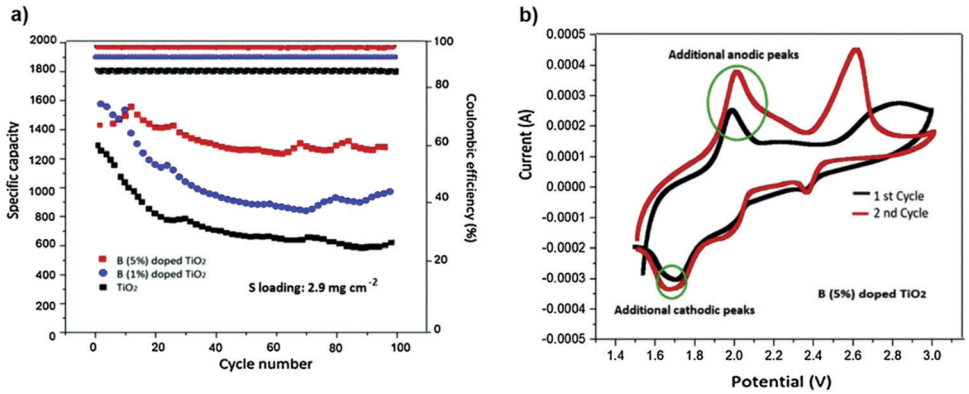

Fig. 26 (a) Cycling performance and coulombic efficiency of Li–S cells for three different coatings at 1 C. (b) First two CV curves of the cell with a 5% B-doped TiO_2 coating swept at 0.1 mV s^{-1}. Image reprinted with the permission from ref. 140. Copyright © 2020, Elsevier License 5040720744337.

SEI layer on the surface of the Li anode. This protective layer effectively restrains the shuttle effect of polysulfides and self-discharging. Subsequently, a $LiNO_3$-containing ether electrolyte could improve the cycling performance and stability in Li–S batteries.[141,142] In another study, the contribution of $LiNO_3$ and polysulfides was investigated as additives to the ether electrolyte, and the results showed the equally important role of both additives to form an SEI film to suppress the shuttle effect. This SEI film consists of two sub-layers. The top layer includes the oxidized products of polysulfides, and the bottom layer consists of the reduced products of polysulfides and $LiNO_3$. This suggests that the presence of $LiNO_3$ and polysulfides in the electrolyte could provide a different structure for the SEI film and lead to significantly low impedance for Li-ion transfer through the SEI film[143] (Fig. 27).

LiTFSI and 0.5 M $LiNO_3$ in a solvent mixture of DOL and DME with a novel Fe-doped TiO_2 coating on the separator have been developed to enhance the Li–S battery performance. The cell with a 5 wt% Fe-doped separator and a $LiNO_3$-containing ether electrolyte showed a low-capacity decay rate of 0.08% per cycle with a superior capacity retention of 751 mA h g^{-1} after 500 cycles at 1 C. The polarization potential value for 5% Fe-doped TiO_2 was as small as 221 mV. Additionally, the value of the polarization potential was maintained as the number of cycles was increased[144] (Fig. 28).

Fluorinated ether has been suggested recently as a novel ether electrolyte that has a low viscosity, low flammability and stronger electronegative ability as a promising additive for Li–S electrolytes. Fluorinated ethers could alleviate the dissolution and diffusion of polysulfides into the electrolyte. The fluorinated

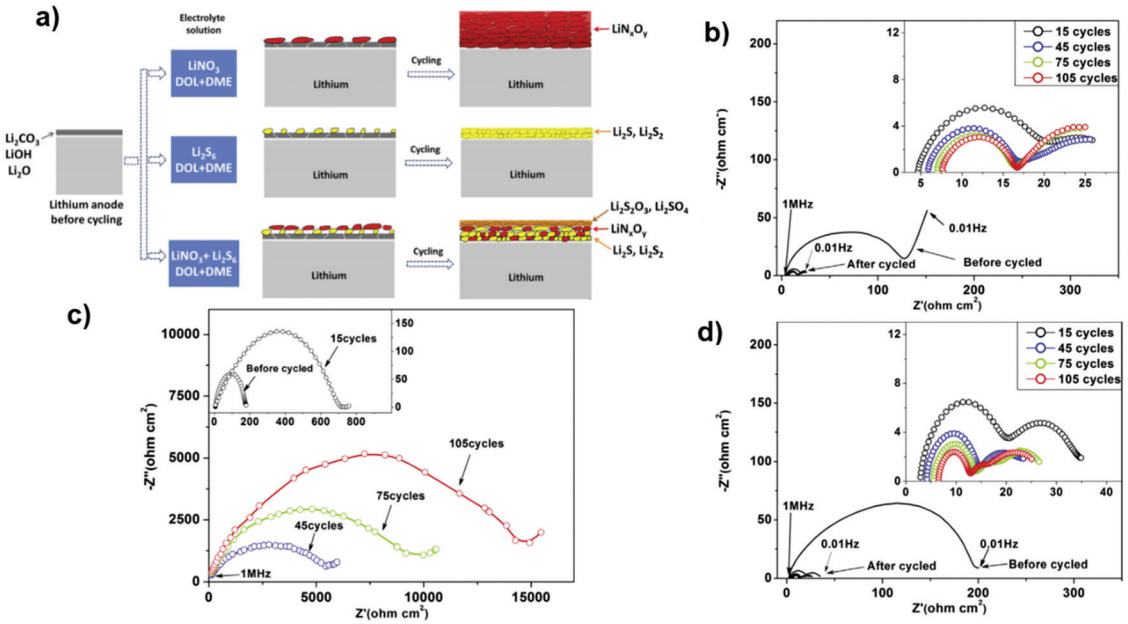

Fig. 27 (a) Illustration of the surface film behavior on lithium anode cycling in different electrolyte solutions. Impedance spectra from the symmetrical cells containing (b) 0.2 M Li_2S_6/DIOX/DME, (c) 0.2 M $LiNO_3$/DIOX/DME and (d) 0.1 M $LiNO_3$/0.1 M Li_2S_6/DIOX/DME. Image reprinted with the permission from ref. 143. Copyright © 2014, Elsevier License 5041340287373.

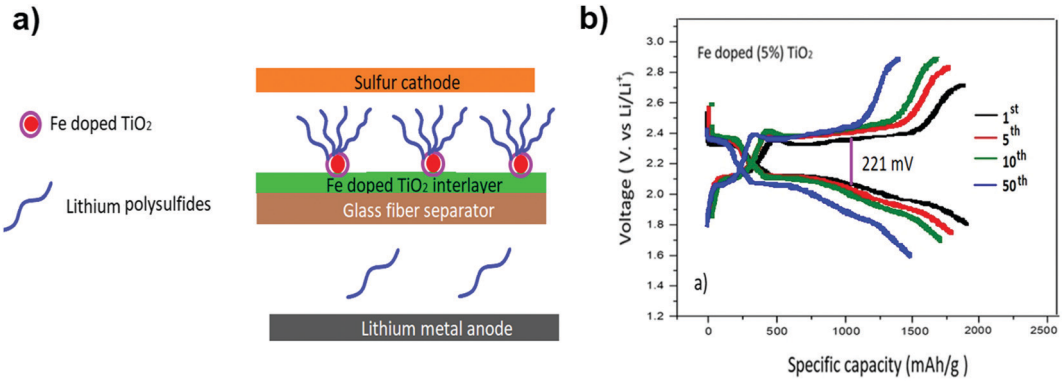

Fig. 28 (a) Schematic for the Li–S battery configuration with the Fe-doped TiO_2 interlayer on a glass fiber separator. (b) Discharge–charge voltage profiles of the Li–S cell with a 5% Fe-doped TiO_2 separator at 1 C. Image reprinted with the permission from ref. 144. Copyright © 2020, Elsevier License 5041340812636.

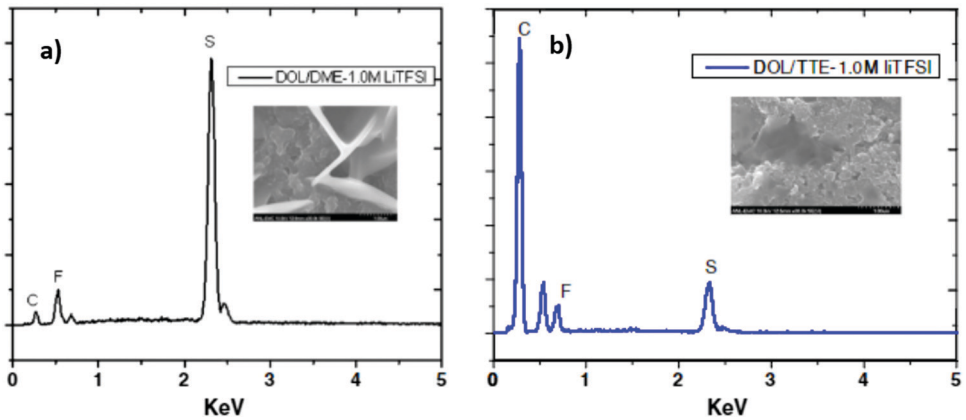

Fig. 29 EDS spectra of the sulfur electrode at the first discharge using (a) 1.0 M LiTFSI DOL/DME and (b) 1.0 M LiTFSI DOL/TTE electrolytes. Image reprinted with the permission from ref. 147. Copyright © 2013, Elsevier License 5041341180684.

ether could enhance the cell performance through the formation of passivation layers on the surfaces of both the Li anode and the sulfur composite cathode.[145,146] Compared with the Li–S cell using the common electrolyte of 1.0 M LiTFSI DOL/DME (5/5), the fluorinated electrolyte cell (TTE) showed a much higher capacity due to the low viscosity and low conductivity of the fluorinated electrolyte. Energy-dispersive X-ray spectroscopy (EDS) revealed a high sulfur signal, as shown in Fig. 29a. However, when using the DOL/TTE fluorinated electrolyte, much less lithium polysulfide deposition was observed in Fig. 29b. Another highly attractive additive to the fluorinated electrolyte is $LiNO_3$, which could suppress self-discharging caused by the reaction of the lithium metal anode with the polysulfide in the electrolyte.[147]

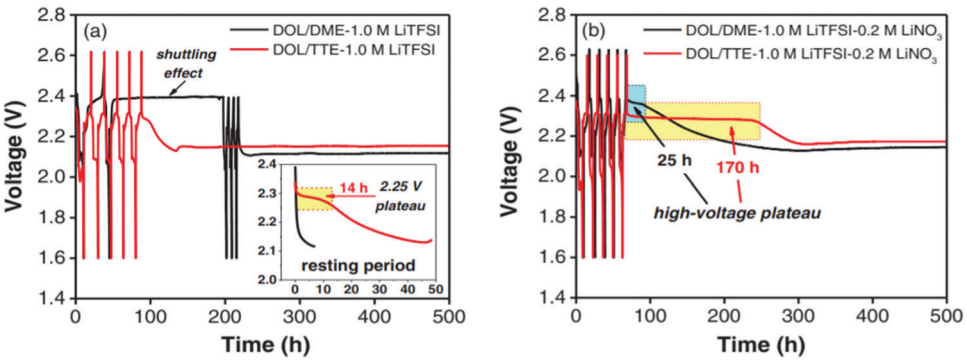

Fig. 30 Voltage profile for Li–S cells rested for an extended period of time with DOL/DME–1.0 M LiTFSI and DOL/TTE–1.0 M LiTFSI (a) without $LiNO_3$ and (b) with 0.2 M $LiNO_3$. Image reprinted with permission from ref. 148. Copyright © 2014, IOP publishing, *J. Electrochem. Soc.*

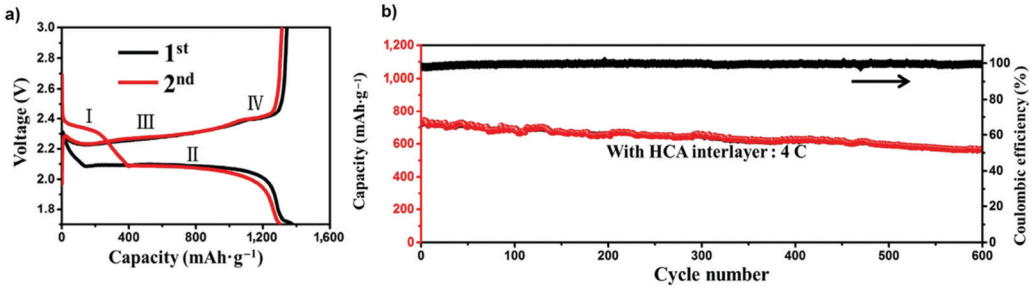

Fig. 31 (a) Charge/discharge curves for the first two cycles of Li–S batteries at 0.2 C. (b) Long-term cycling performance along with the corresponding coulombic efficiency of the Li–S battery at 4 C. Image reprinted with permission from ref. 151. https://doi.org/10.1007/s12274-016-1244-1.

To investigate the effect of the self-discharge-suppressing behavior of the fluoroether solvent, Zhang *et al.* studied the preparation of an electrolyte containing DME/DOL, LiTFSI and $LiNO_3$ with 1,1,2,2-tetrafluoroethyl-2,2,3,3-tetrafluoropropyl ether (TTE). The solvents were dried over activated 4 Å molecular sieves for 24 hours and purified by fractional distillation. The cell containing the DOL/DME–1.0 M LiTFSI electrolyte without the $LiNO_3$ additive showed severe shuttling during the 1st and 2nd charges. The best performance in suppressing self-discharge belongs to the cell containing DOL/TTE–1.0 M LiTFSI with 0.2 M $LiNO_3$. The $LiNO_3$-containing fluoroether provides a protective layer on the Li surface, which could effectively suppress the LiPS diffusion[148] (Fig. 30).

An integrated carbon–sulfur membrane or robust 3D graphene-wrapped, nitrogen-doped, carbon/sulfur aerogel was studied recently with additives including an ether electrolyte.[149,150] Peng *et al.* investigated 1 M LiTFSI in DOL/DME, at a 1 : 1 volume ratio, and 0.1 M $LiNO_3$ as the electrolyte and a conductive hybrid carbon aerogel (HCA). The charge/discharge curves of the Li–S batteries with the HCA interlayers showed two apparent reduction plateaus (I and II in Fig. 31) corresponding to the reduction of S_8 to long-chain polysulfides (Li_2S_n, $4 \leq n \leq 8$) and subsequent reduction to solid Li_2S_2/Li_2S. Two plateaus (III and IV) were found, leading to the reverse reaction from Li_2S/Li_2S_2 to Li_2S_4 and the oxidation of Li_2S_4 to Li_2S_8/S, respectively.[151] The Li–S battery with the HCA interlayer and $LiNO_3$ including the ether electrolyte was subjected to a 600-cycle long-term test at a high current density of 4 C, and exhibited a specific capacity of 597 mA h g^{-1} with a coulombic efficiency of 100%, where the specific capacity decayed at a rate of just 0.037% per cycle.

7. Conclusion and outlook

In this review, recent advances in electrolytes ranging from liquids (carbonates, ethers, and ionic liquid electrolyte) to solids (polymer and inorganic electrolytes) and also novel electrolytes have been studied. The advantages and limitations of various electrolytes for Li–S batteries are summarized in Table 1. Recent research has shown that certain electrolyte additives and solid-based electrolytes can reduce polysulfide solubility, thereby improving the capacity, coulombic efficiency, cycling ability, and cell life. Electrolyte design was investigated in two different designs: (1) polysulfide-solubilized and (2) polysulfide-insolubilized. Both designs have their own advantages and disadvantages, and it is not possible to determine a specific electrolyte for practical Li–S batteries. Polysulfide-solubilized designs allowed dissolved polysulfides to access to the electrode. But to avoid electrolyte instability, additives should be used to alleviate low-order polysulfide precipitation. In Li–S cells with a polysulfide-insolubilized design, the dissolution of the active species can be hindered, resulting in a high coulombic efficiency and a long cycling life. These electrolytes are highly viscous and have a low ion conductivity, which may affect ion transport. The addition of low-polar solvents could improve the transport properties. As a matter of fact, liquid electrolytes with a high ionic conductivity have some drawbacks, such as lithium dendrite formation, polysulfide dissolution and shuttle effects. Adding a suitable amount of conductive organic modifier to pure liquid electrolytes results in a higher and more stable capacity. DOL can increase the electrode/electrolyte interfacial properties, and DME modifies the PS solubility, and thus a different proportion of DOL/DME increases the battery performance. In most cases, the higher the DOL content, the faster the capacity drops. In the presence of a higher percentage of DME, both the conductivity and capacity rise. The capacity is also increased by using a modified amount of the additive.

Ionic-liquid electrolytes, with a high ionic conductivity and high protection of the lithium metal anode, have some drawbacks such as easy evaporation and undesirable by-products with polysulfides. Because of the difference in viscosity and Li ion transportation, ionic-liquid cations can impact the battery capacity. Polysulfide solubility is suppressed by solvate ionic liquids, resulting in a battery with a stable capacity. Solid electrolytes effectively restrain the dissolution of polysulfides and form effective solid–electrolyte/solid–electrode interfaces for facile electrochemical reactions. On the other hand, the solid-based electrolyte increases the cell polarization due to sluggish electrochemical reactions. Further investigations into the reactions between sulfur and solid-based electrolytes should be carried out to understand the redox reactions on the surface of the solid electrolytes and improve the interface properties. The composition of the organic solvent has an impact on the polymer-electrolyte performance. While solid electrolytes effectively prevent lithium polysulfide

Table 1 Characteristics of different electrolytes in Li–S batteries

Electrolyte	Typical example	Advantages	Drawbacks
Carbonate solvents	$LiPF_6$/EC + DEC	• High dielectric constant • Low viscosity	• Sever capacity fading • Incompatible with polysulfides
Ether solvents	LiTFSI in DOL/DME	• Stable toward polysulfides • Low viscosity • High conductivity • High polysulfide solubility	• Lithium dendrite formation • Polysulfides diffusion • Easy evaporation • Severe shuttle effect
Ionic liquid-electrolytes	*N*-Methyl-*N*-butylpiperidinium (PP14) bis(trifluoromethanesulfonyl)imide (TFSI)	• Acceptable electro-chemical stability • Wider liquid temperature range • High conductivity • Suppressed shuttle effect • Improving the safety	• Easy evaporation • Undesirable by-products with polysulfides • Low conductivity • Slow Li^+ transport
Polymer electrolytes	$PEO_{18}Li(CF_3SO_2)_2N–SiO_2$	• Solvent-free • High mechanical stability • Prevention of Li dendrite formation • High ionic conductivity • Excellent mechanical integrity	• High cell polarization • Low conductivity • Complicated redox reactions • Poor rate capability
Inorganic solid electrolytes	Thio-LISICON $Li_{3.25}Ge_{0.25}P_{0.75}S_4$	• High ionic conductivity • Excellent interface compatibility • Wide electrochemical window	• Low conductivity • Sluggish electrochemical reaction • High cell polarization
Novel hybrid electrolytes	$Li[N(SO_2F)_2]$ and $Li[N(SO_2CF_3)_2]$	• High conductivity • Mechanically stable • Less lithium dendrite • Protect the Li anode	• High viscosity • Sluggish electrochemical reaction • Poor rate capability

dissolution, there are still many obstacles to be overcome in terms of appropriate conductivities for ambient-temperature operation for facile electrochemical reactions. Novel or conducting polymer solid electrolytes could enhance the conductivity and interface stability, but their high viscosity may cause capacity fading. As a result, the selection of functional and hybrid electrolytes must be developed in tandem with the selection of cathode materials in order to achieve a higher energy density and excellent stability in Li–S batteries.

Conflicts of interest

The authors declare no conflicts of interest.

Acknowledgements

Dr Maryam Sadat Kiai would like to thank Istanbul Technical University-Istanbul for financial support of this work. Also would like to thank Andhra University College of Engineering, Andhra University, Visakhapatnam-India and Indian Institute of Science-Bangalore, India for resource support. Srikanth Ponnada and Dr Annapurna Nowduri would like to thank Andhra University College of Engineering, Andhra University, Visakhapatnam-India, Indian Institute of Science-Bangalore and Istanbul Technical University-Istanbul for resource and technical support. Dr Demudu Babu Gorle would like to thank Indian Institute of Science Bangalore, University Grants Commission and Government of India for providing Dr D. S. Kothari Postdoctoral Fellowship, Andhra University College of Engineering, Andhra University, Visakhapatnam-India and Istanbul Technical University-Turkey.

References

1 M. Hagen, D. Hanselmann, K. Ahlbrecht, R. Maça, D. Gerber and J. Tübke, Lithium–sulfur cells: The gap between the state-of-the-art and the requirements for high energy battery cells, *Adv. Energy Mater.*, 2015, **5**, 1401986.
2 A. Manthiram, Y. Fu and Y. S. Su, Challenges and prospects of lithium–sulfur batteries, *Acc. Chem. Res.*, 2013, **46**, 1125–1134.
3 G. Xu, B. Ding, J. Pan, P. Nie, L. Shen and X. Zhang, High performance lithium–sulfur batteries: Advances and challenges, *J. Mater. Chem. A*, 2014, **2**, 12662–12676.
4 Y. Z. Zhang, Z. Zhang, S. Liu, G. R. LiX and P. Gao, Free-standing porous carbon nanofiber/carbon nanotube film as sulfur immobilizer with high areal capacity for lithium–sulfur battery, *ACS Appl. Mater. Interfaces*, 2018, **10**, 8749–8757.
5 N. Jayaprakash, J. Shen, S. S. Moganty, A. Corona and L. A. Archer, Porous hollow carbon@sulfur composites for high-power lithium–sulfur batteries, *Angew. Chem., Int. Ed.*, 2011, **50**, 5904–5908.
6 S. Moon, Y. H. Jung, W. K. Jung, D. S. Jung, J. W. Choi and D. K. Kim, Encapsulated monoclinic sulfur for stable cycling of Li–S rechargeable batteries, *Adv. Mater.*, 2013, **25**, 65476553.
7 X. Q. Zhang, B. He, W. C. Li and A. H. Lu, Hollow carbon nanofibers with dynamic adjustable pore sizes and closed ends as hosts for high-rate lithium–sulfur battery cathodes, Nano, *Research*, 2018, **11**, 1238–1246.
8 H. Wu, L. Xia, J. Ren, Q. Zheng, C. Xu and D. Lin, A high-efficiency N/P co-doped graphene/CNT@ porous carbon hybrid matrix as a cathode host for high performance

lithium–sulfur batteries, *J. Mater. Chem. A*, 2017, **5**, 20458–20472.

9 A. A. Arie, H. Kristianto, E. C. Cengiz and R. Demir-Cakan, activated porous carbons originated from the Indonesian snake skin fruit peel as cathode components for lithium sulfur battery, *Ionics*, 2019, **25**, 2121–2129.

10 S. Wu, R. Ge, M. Lu, R. Xu and Z. Zhang, Graphene-based nano-materials for lithium–sulfur battery and sodium-ion battery, *Nano Energy*, 2015, **15**, 379–405.

11 T. Lin, Y. Tang, Y. Wang, H. Bi, Z. Liu, F. Huang, X. Xie and M. Jiang, Scotch-tape-like exfoliation of graphite assisted with elemental sulfur and graphene–sulfur composites for high-performance lithium–sulfur batteries, *Energy Environ. Sci.*, 2013, **6**, 1283–1290.

12 M. S. Kiai and H. Kizil, Enhanced performance of Li–S battery with polymer doped potassium functionalized graphene interlayers as effective polysulfide barrier, *J. Electroanal. Chem.*, 2019, **851**, 113405.

13 M. S. Kiai, O. Eroglu and H. Kizil, Polycarboxylate functionalized graphene/S composite cathodes and modified cathode-facing side coated separators for advanced lithium–sulfur batteries, *Nanoscale Res. Lett.*, 2019, **4**, 1–11.

14 G. Xu, Q. B. Yan, A. Kushima, X. Zhang, J. Pan and J. Li, Conductive graphene oxide-polyacrylic acid (GOPAA) binder for lithium–sulfur battery, *Nano Energy*, 2017, **31**, 568–574.

15 X. Yao, N. Huang, F. Han, Q. Zhang, H. Wan, J. P. Mwizerwa and X. Xu, High-performance all-solid-state lithium–sulfur batteries enabled by amorphous sulfur-coated reduced graphene oxide cathodes, *Adv. Energy Mater.*, 2017, **7**, 1602923.

16 J. M. Chabu, K. Zeng, W. Chen, A. Mustapha, Y. Li and Y. N. Liu, A novel graphene oxide-wrapped sulfur composites cathode with ultra-high sulfur content for lithium–sulfur battery, *Appl. Surf. Sci.*, 2019, **493**, 533–540.

17 A. B. Puthirath, A. Baburaj, K. Kato, D. Salpekar, N. Chakingal, Y. Cao, G. Babu and P. M. Ajayan, High sulfur content multifunctional conducting polymer composite electrodes for stable Li–S battery, *Electrochim. Acta*, 2019, **306**, 489–497.

18 S. Zeng, L. Li, L. Xie, D. Zhao, N. Wang and S. Chen, Conducting polymers crosslinked with sulfur as cathode materials for high-rate, Ultralong-life lithium–sulfur batteries, *ChemSusChem*, 2017, **10**, 3378–3386.

19 G. Ma, F. Huang, Z. Wen, Q. Wang, X. Hong, J. Jin and X. Wu, Enhanced performance of lithium sulfur batteries with conductive polymer modified separators, *J. Mater. Chem. A*, 2016, **4**, 16968–16974.

20 S. Dai, Y. Feng, P. Wang, H. Wang, H. Liang, R. Wang and S. Ji, Highly conductive copolymer/sulfur composites with covalently grafted polyaniline for stable and durable lithium–sulfur batteries, *Electrochim. Acta*, 2019, **321**, 134678.

21 M. S. Kiai, O. Eroglu and H. Kizil, Electrospun nanofiber polyacrylonitrile coated separators to suppress the shuttle effect for long-life lithium–sulfur battery, *J. Appl. Polym. Sci.*, 2020, **137**, 48606.

22 J. Li, Y. Huang, S. Zhang, W. Jia, X. Wang, Y. Guo and L. Wang, Decoration of silica nanoparticles on polypropylene separator for lithium–sulfur batteries, *ACS Appl. Mater. Interfaces*, 2017, **9**, 7499–7504.

23 J. Zhang, P. Gu, J. Xu, H. Xue and H. Pang, High performance of electrochemical lithium storage batteries: ZnO-based nanomaterials for lithium-ion and lithium–sulfur batteries, *Nanoscale*, 2016, **8**, 18578–18595.

24 P. Jia, T. Hu, Q. He, X. Cao, J. Ma, J. Fan and J. Geng, Synthesis of a macroporous conjugated polymer framework: Iron doping for highly stable, highly efficient lithium–sulfur batteries, *ACS Appl. Mater. Interfaces*, 2018, **11**, 3087–3097.

25 S. Luo, W. Sun, J. Ke, Y. Wang, S. Liu, X. Hong, Y. Li, Y. Chen, W. Xie and C. Zheng, A 3D conductive network of porous carbon nanoparticles interconnected with carbon nanotubes as the sulfur host for long cycle life lithium–sulfur batteries, *Nanoscale*, 2018, **10**, 22601–22611.

26 X. Li, M. Rao and W. Li, Sulfur encapsulated in porous carbon nanospheres and coated with conductive polyaniline as cathode of lithium–sulfur battery, *J. Solid. State Electron.*, 2016, **20**, 153–161.

27 Q. Pang, X. Liang, C. Y. Kwok and L. F. Nazar, Advances in lithium–sulfur batteries based on multifunctional cathodes and electrolytes, *Nat. Energy*, 2016, **1**, 1–11.

28 Z. Zhang, L. L. Kong, S. Liu, G. R. Li and X. P. Gao, A high-efficiency sulfur/carbon composite based on 3D graphene nanosheet@carbon nanotube matrix as cathode for lithium–sulfur battery, *Adv. Energy Mater.*, 2017, **7**, 1602543.

29 J. Scheers, S. Fantini and P. Johansson, A review of electrolytes for lithium–sulphur batteries, *J. Power Sources*, 2014, **255**, 204–218.

30 D. Zhou, M. Liu, Q. Yun, X. Wang, Y. B. He, B. Li, Q. H. Yang, Q. Cai and F. Kang, A novel lithiated silicon–sulfur battery exploiting an optimized solid-like electrolyte to enhance safety and cycle life, *Small*, 2017, **13**, 1602015.

31 S. Xiong, M. Regula, D. Wang and J. Song, Toward better lithium–sulfur batteries: Functional non-aqueous liquid electrolytes, *Electrochem. Energy Rev.*, 2018, **1**, 388–402.

32 W. Chen, T. Lei, C. Wu, M. Deng, C. Gong, K. Hu, Y. Ma, L. Dai, W. Lv, W. He and X. Liu, Designing safe electrolyte systems for a high-stability lithium–sulfur battery, *Adv. Energy Mater.*, 2018, **8**, 1702348.

33 S. Xiong, K. Xie, E. Blomberg, P. Jacobsson and A. Matic, Analysis of the solid electrolyte interphase formed with an ionic liquid electrolyte for lithium–sulfur batteries, *J. Power Sources*, 2014, **252**, 150–155.

34 J. Gao, M. A. Lowe, Y. Kiya and H. D. Abruña, Effects of liquid electrolytes on the charge–discharge performance of rechargeable lithium/sulfur batteries: Electrochemical and *in situ* X-ray absorption spectroscopic studies, *J. Phys. Chem. C*, 2011, **115**, 25132–25137.

35 T. Yim, M.-S. Park, J.-S. Yu, K. J. Kim, K. Y. Im, J.-H. Kim, G. Jeong, Y. N. Jo, S.-G. Woo and K. S. Kang, Effect of chemical reactivity of polysulfide toward carbonate-based electrolyte on the electrochemical performance of Li–S batteries, *Electrochim. Acta*, 2013, **107**, 454–460.

36 S. Niu, G. Zhou, W. Lv, H. Shi, C. Luo, Y. He, B. Li, Q. H. Yang and F. Kang, Sulfur confined in nitrogen-doped microporous carbon used in a carbonate-based electrolyte for long-life, safe lithium–sulfur batteries, *Carbon*, 2016, **109**, 1–6.

37 S. Zheng, P. Han, Z. Han, H. Zhang, Z. Tang and J. Yang, High performance C/S composite cathodes with conventional carbonate-based electrolytes in Li–S battery, *Sci. Rep.*, 2014, **4**, 1–7.

38 Z. Zhang, Z. Li, F. Hao, X. Wang, Q. Li, Y. Qi, R. Fan and L. Yin, 3D interconnected porous carbon aerogels as sulfur immobilizers for sulfur impregnation for lithium–sulfur batteries with high-rate capability and cycling stability, *Adv. Funct. Mater.*, 2014, **24**, 2500–2509.

39 X. Li, M. Banis, A. Lushington, X. Yang, Q. Sun, Y. Zhao, C. Liu, Q. Li, B. Wang, W. Xiao and C. Wang, A high-energy sulfur cathode in carbonate electrolyte by eliminating polysulfides *via* solid-phase lithium–sulfur transformation, *Nat. Commun.*, 2018, **9**, 1–10.

40 J. Ma, G. Xu, Y. Li, C. Ge and X. Li, An in situ chemically and physically confined sulfur–polymer composite for lithium–sulfur batteries with carbonate-based electrolytes, *Chem. Commun.*, 2018, **54**, 14093–14096.

41 S. Zheng, Y. Chen, Y. Xu, F. Yi, Y. Zhu, Y. Liu, J. Yang and C. Wang, in situ formed lithium sulfide/microporous carbon cathodes for lithium-ion batteries, *ACS Nano*, 2013, **7**, 10995–11003.

42 L. Hu, Y. Lu, X. Li, J. Liang, T. Huang, Y. Zhu and Y. Qian, Optimization of microporous carbon structures for lithium–sulfur battery applications in carbonate-based electrolyte, *Small*, 2017, **13**, 1603533.

43 S. S. Zhang, Understanding of sulfurized polyacrylonitrile for superior performance lithium/sulfur battery, *Energies*, 2014, **7**, 4588–4600.

44 S. S. Zhang, Status, opportunities, and challenges of electrochemical energy storage, *Front. Energy Res.*, 2013, **1**, 8.

45 J. Ma, G. Xu, Y. Li, C. Ge and X. Li, An in situ chemically and physically confined sulfur–polymer composite for lithium–sulfur batteries with carbonate-based electrolytes, *Chem. Commun.*, 2018, **54**, 14093–14096.

46 G. Li, Z. Li, B. Zhang and Z. Lin, Developments of electrolyte systems for lithium–sulfur batteries: A review, *Front. Energy Res.*, 2015, **3**, 5.

47 K. Jeddi, K. Sarikhani, N. T. Qazvini and P. Chen, Stabilizing lithium/sulfur batteries by a composite polymer electrolyte containing mesoporous silica particles, *J. Power Sources*, 2014, **245**, 656–662.

48 A. Konarov, D. Gosselink, T. N. L. Doan, Y. Zhang, Y. Zhao and P. Chen, Simple, scalable, and economical preparation of sulfur–PAN composite cathodes for Li/S batteries, *J. Power Sources*, 2014, **259**, 183–187.

49 L. Wang, X. He, J. Li, M. Chen, J. Gao and C. Jiang, Charge/discharge characteristics of sulfurized polyacrylonitrile composite with different sulfur content in carbonate based electrolyte for lithium batteries, *Electrochim. Acta*, 2012, **72**, 114–119.

50 B. Wu, Q. Liu, D. Mu, Y. Ren, Y. Li, L. Wang and F. Wu, New desolvated gel electrolyte for rechargeable lithium metal sulfurized polyacrylonitrile (S-PAN) battery, *J. Phys. Chem. C*, 2014, **118**, 28369–28376.

51 P. Zeng, Y. Han, X. Duan, G. Jia, L. Huang and Y. Chen, A stable graphite electrode in superconcentrated LiTFSI-DME/DOL electrolyte and its application in lithium–sulfur full battery, *Mater. Res. Bull.*, 2017, **95**, 61–70.

52 S. S. Zhang, New insight into liquid electrolyte of rechargeable lithium/sulfur battery, *Electrochim. Acta*, 2013, **97**, 226–230.

53 H. Ryu, H. Ahn, K. Kim, J. Ahn, K. Cho and T. Nam, Self-discharge characteristics of lithium/sulfur batteries using TEGDME liquid electrolyte, *Electrochim. Acta*, 2006, **52**, 1563–1566.

54 H.-S. Ryu, H.-J. Ahn, K.-W. Kim, J.-H. Ahn, K.-K. Cho, T.-H. Nam, J.-U. Kim and G.-B. Cho, Discharge behavior of lithium/sulfur cell with TEGDME based electrolyte at low temperature, *J. Power Sources*, 2006, **163**, 201–206.

55 H. S. Kim, T. G. Jeong, N. S. Choi and Y. T. Kim, The cycling performances of lithium–sulfur batteries in TEGDME/DOL containing $LiNO_3$ additive, *Ionics*, 2013, **19**, 1795–1802.

56 J. W. Choi, G. Cheruvally, D. S. Kim, J. H. Ahn, K. W. Kim and H. J. Ahn, Rechargeable lithium/sulfur battery with liquid electrolytes containing toluene as additive, *J. Power Sources*, 2008, **183**, 441–445.

57 C. Barchasz, J.-C. Leprêtre, S. Patoux and F. Alloin, Electrochemical properties of ether-based electrolytes for lithium/sulfur rechargeable batteries, *Electrochim. Acta*, 2013, **89**, 737–743.

58 Y.-X. Wang, S.-L. Chou, H.-K. Liu and S.-X. Dou, Electrochemical properties of high-capacity sulfur/reduced graphene oxide with different electrolyte systems, *J. Power Sources*, 2013, **244**, 240–245.

59 C. Qu, Y. Chen, X. Yang, H. Zhang, X. Li and H. Zhang, $LiNO_3$-free electrolyte for Li–S battery: A solvent of choice with low Ksp of polysulfide and low dendrite of lithium, *Nano Energy*, 2017, **39**, 262–272.

60 J. Qian, W. A. Henderson, W. Xu, P. Bhattacharya, M. Engelhard, O. Borodin and J. G. Zhang, High rate and stable cycling of lithium metal anode, *Nat. Commun.*, 2015, **6**, 6362.

61 J. Zhou, Y. Guo, C. Liang, L. Cao, H. Pan, J. Yang and J. Wang, A new ether-based electrolyte for lithium sulfur batteries using a S@pPAN cathode, *Chem. Commun.*, 2018, **54**, 5478–5481.

62 Q. J. Meisner, T. Rojas, N. L. D. Rago, J. Cao, T. Glossmann, A. Hintennach, P. C. Redfern, D. Pahls, L. Zhang and I. D. Bloom, Lithium–sulfur battery with partially fluorinated ether electrolytes: Interplay between capacity, coulombic efficiency and Li anode protection, *J. Power Sources*, 2019, **438**, 226939.

63 X. Wang, Y. Tan, G. Shen and S. Zhang, Recent progress in fluorinated electrolytes for improving the performance of Li–S batteries, *J. Energy Chem.*, 2020, **41**, 149.

64 N. Azimi, Z. Xue, I. Bloom, M. L. Gordin, D. Wang, T. Daniel, C. Takoudis and Z. Zhang, Understanding the

effect of a fluorinated ether on the performance of lithium–sulfur batteries, *ACS Appl. Mater. Interfaces*, 2015, **7**, 9169.

65 M. L. Gordin, F. Dai, S. Chen, T. Xu, J. Song, D. Tang, N. Azimi, Z. Zhang and D. Wang, Bis(2,2,2-trifluoroethyl)ether as an electrolyte co-solvent for mitigating self-discharge in lithium–sulfur batteries, *ACS Appl. Mater. Interfaces*, 2014, **6**, 8006.

66 C. Zu, N. Azimi, Z. Zhang and A. Manthiram, Insight into lithium–metal anodes in lithium–sulfur batteries with a fluorinated ether electrolyte, *J. Mater. Chem. A*, 2015, **3**, 14864.

67 S. Drvaric Talian, S. Jeschke, A. Vizintin, K. Pirnat, I. Arcon, G. Aquilanti, P. Johansson and R. Dominko, Fluorinated ether based electrolyte for high-energy lithium–sulfur batteries: Li^+ solvation role behind reduced polysulfide solubility, *Chem. Mater.*, 2017, **29**, 10037.

68 W. J. Chen, C. X. Zhao, B. Q. Li, Q. Jin, X. Q. Zhang, T. Q. Yuan, X. Zhang, Z. Jin, S. Kaskel and Q. Zhang, A mixed ether electrolyte for lithium metal anode protection in working lithium–sulfur batteries, *Energy Environ. Mater.*, 2020, **3**, 160–165.

69 K. Ueno, J. W. Park, A. Yamazaki, T. Mandai, N. Tachikawa, K. Dokko and M. Watanabe, Anionic effects on solvate ionic liquid electrolytes in rechargeable lithium–sulfur batteries, *J. Phys. Chem. C*, 2013, **117**, 20509–20516.

70 S. Zhang, K. Ueno, K. Dokko and M. Watanabe, Recent advances in electrolytes for lithium–sulfur batteries, *Adv. Energy Mater.*, 2015, **5**, 1500117.

71 L. X. Yuan, J. Feng, X. P. Ai, Y. L. Cao, S. L. Chen and H. X. Yang, Improved dischargeability and reversibility of sulfur cathode in a novel ionic liquid electrolyte, *Electrochem. Commun.*, 2006, **8**, 610–614.

72 C. Zhang, K. Ueno, A. Yamazaki, K. Yoshida, H. Moon, T. Mandai and M. Watanabe, chelate effects in glyme/lithium bis(trifluoromethanesulfonyl)amide solvate ionic liquids. I. Stability of solvate cations and correlation with electrolyte properties, *J. Phys. Chem. B*, 2014, **118**, 5144–5153.

73 C. Zhang, A. Yamazaki, J. Murai, J. W. Park, T. Mandai, K. Ueno and M. Watanabe, Chelate effects in glyme/lithium bis (trifluoromethanesulfonyl) amide solvate ionic liquids, part 2: Importance of solvate-structure stability for electrolytes of lithium batteries, *J. Phys. Chem. C*, 2014, **118**, 17362–17373.

74 L. Wang and H. R. Byon, *N*-Methyl-*N*-propylpiperidinium bis(trifluoromethanesulfonyl)imide-based organic electrolyte for high performance lithium–sulfur batteries, *J. Power Sources*, 2013, **236**, 207–214.

75 M. Barghamadi, A. S. Best and A. I. Bhatt, Effect of anion on behaviour of Li–S battery electrolyte solutions based on *N*-methyl-*N*-butyl-pyrrolidinium ionic liquids, *Electrochim. Acta*, 2015, **180**, 636–644.

76 F. Wu, Q. Zhu, R. Chen, N. Chen, Y. Chen, Y. Ye and L. Li, Ionic liquid-based electrolyte with binary lithium salts for high performance lithium–sulfur batteries, *J. Power Sources*, 2015, **296**, 10–17.

77 Y. Wang, Z. Zhang, M. Haibara, D. Sun, X. Ma, Y. Jin, H. Munakata and K. Kanamura, Reduced polysulfide shuttle effect by using polyimide separators with ionic liquid-based electrolytes in lithium–sulfur battery, *Electrochim. Acta*, 2017, **255**, 109–117.

78 W. Kang, N. Deng, J. Ju, Q. Li, D. Wu, X. Ma and B. Cheng, A review of recent developments in rechargeable lithium–sulfur batteries, *Nanoscale*, 2016, **8**, 16541–16588.

79 A. Unemoto, H. Ogawa, Y. Gambe and I. Honma, Development of lithium–sulfur batteries using room temperature ionic liquid-based quasi-solid-state electrolytes, *Electrochim. Acta*, 2014, **125**, 386–394.

80 A. Manthiram, X. Yu and S. Wang, Lithium battery chemistries enabled by solid-state electrolytes, *Nat. Rev. Mater.*, 2017, **2**, 1–16.

81 J. Janek and W. G. Zeier, A solid future for battery development, *Nat. Energy*, 2016, **1**, 1–4.

82 Y. X. Xiang, G. Zheng and G. Zhong, D. Wang. R. Fu. Y. Yang, toward understanding of ion dynamics in highly conductive lithium-ion conductors: some perspectives by solid state NMR techniques, *Solid State Ionics*, 2018, **318**, 19–26.

83 K. K. Fu, Y. Gong, S. Xu, Y. Zhu, Y. Li, J. Dai, G. Pastel, H. Xie and Y. Yao, Stabilizing the garnet solid-electrolyte/polysulfide interface in Li–S batteries, *Chem. Mater.*, 2017, **29**, 8037–8041.

84 Y. Lin, X. Wang, J. Liu and J. D. Miller, Natural halloysite nano-clay electrolyte for advanced all-solid-state lithium–sulfur batteries, *Nano Energy*, 2017, **31**, 478–485.

85 L. Chen and Z. Fan, Dendrite-free Li metal deposition in all-solid-state lithium sulfur batteries with polymer-in-salt polysiloxane electrolyte, *Energy Storage Mater.*, 2018, **15**, 37–45.

86 X. Judez, H. Zhang, C. Li, G. G. Eshetu, Y. Zhang, J. A. González-Marcos, M. Armand and L. M. Rodriguez-Martinez, Polymer-rich composite electrolytes for all-solid-state Li–S cells, *J. Phys. Chem. Lett.*, 2017, **8**, 3473–3477.

87 Y. Takeda, O. Yamamoto and N. Imanishi, Lithium dendrite formation on a lithium metal anode from liquid, polymer and solid electrolytes, *Electrochemistry*, 2016, **84**, 210–218.

88 J. Hassoun and B. Scrosati, Moving to a solid-state configuration: a valid approach to making lithium–sulfur batteries viable for practical applications, *Adv. Mater.*, 2010, **22**, 5198–5201.

89 C. Zhang, Y. Lin and J. Liu, Sulfur double locked by a macro-structural cathode and a solid polymer electrolyte for lithium–sulfur batteries, *J. Mater. Chem. A*, 2015, **3**, 10760–10766.

90 H. Marceau, C. S. Kim, A. Paolella, S. Ladouceur, M. Lagacé, M. Chaker, A. Vijh, A. Guerfi, C. M. Julien, A. Mauger and M. Armand, In operando scanning electron microscopy and ultraviolet–visible spectroscopy studies of lithium/sulfur cells using all solid-state polymer electrolyte, *J. Power Sources*, 2016, **319**, 247–254.

91 M. Agostini, Y. Aihara, T. Yamada, B. Scrosati and J. A. Hassoun, A lithium–sulfur battery using a solid, glass-type P_2S_5–Li_2S electrolyte, *Solid State Ionics*, 2013, **244**, 48–51.

92 B. Huang, X. Yao, Z. Huang, Y. Guan, Y. Jin and X. Xu, Li_3PO_4-Doped $Li_7P_3S_{11}$ glass-ceramic electrolytes with enhanced lithium-ion conductivities and application in all-solid-state batteries, *J. Power Sources*, 2015, **284**, 206–211.

93 D. Liu, W. Zhu, Z. Feng, A. Guerfi, A. Vijh and K. Zaghib, Recent progress in sulfide-based solid electrolytes for Li-ion batteries, *Mater. Sci. Eng., B*, 2016, **213**, 169–176.

94 P. Bron, S. Johansson, K. Zick, J. Schmedt auf der Günne, S. Dehnen and B. Roling, $Li_{10}S_nP_2S_{12}$: An affordable lithium superionic conductor, *J. Am. Chem. Soc.*, 2013, **135**, 15694–15697.

95 Y. Kato, S. Hori, T. Saito, K. Suzuki, M. Hirayama, A. Mitsui, M. Yonemura, H. Iba and R. Kanno, High-power all-solid-state batteries using sulfide superionic conductors, *Nat. Energy*, 2016, **1**, 1–7.

96 M. Chen and S. J. Adams, High performance all-solid-state lithium/sulfur batteries using lithium argyrodite electrolyte, *Solid State Electrochem.*, 2015, **19**, 697–702.

97 D. Wang, G. Zhong, W. K. Pang, Z. Guo, Y. Li, M. J. McDonald, R. Fu, J. X. Mi and Y. Yang, toward understanding the lithium transport mechanism in garnet-type solid electrolytes: Li^+ ion exchanges and their mobility at octahedral/tetrahedral sites, *Chem. Mater.*, 2015, **27**, 6650–6659.

98 P. J. Lian, B. S. Zhao, L. Q. Zhang, N. Xu, M. T. Wu and X. P. Gao, Inorganic sulfide solid electrolytes for all-solid-state lithium secondary batteries, *J. Mater. Chem. A*, 2019, **7**, 20540–20557.

99 H. Lee, P. Oh, J. Kim, H. Cha, S. Chae, S. Lee and J. Cho, Advances and prospects of sulfide all-solid-state lithium batteries via one-to-one comparison with conventional liquid lithium ion batteries, *Adv. Mater.*, 2019, **31**, 1900376.

100 X. Liang, Z. Wen, Y. Liu, H. Zhang, L. Huang and J. Jin, highly dispersed sulfur in ordered mesoporous carbon sphere as a composite cathode for rechargeable polymer Li/S battery, *J. Power Sources*, 2011, **196**, 3655–3658.

101 D. Devaux, I. Villaluenga, X. Jiang, Y. H. Chang, D. Y. Parkinson and N. P. Balsara, Lithium–sulfur batteries with a block copolymer electrolyte analyzed by X-ray microtomography, *J. Electrochem. Soc.*, 2020, **167**, 060506.

102 G. M. Stone, S. A. Mullin, A. A. Teran, D. T. Hallinan, A. M. Minor, A. Hexemer and N. P. Balsara, Solid polymer electrolyte composition, *J. Electrochem. Soc.*, 2012, **159**, A222–A227.

103 A. A. Teran and N. P. Balsara, Effect of lithium polysulfides on the morphology of block copolymer electrolytes, *Macromolecules*, 2011, **44**, 9267–9275.

104 J. Jin, Z. Wen, X. Liang, Y. Cui and X. Wu, Gel polymer electrolyte with ionic liquid for high performance lithium sulfur battery, *Solid State Ionics*, 2012, **225**, 604–607.

105 K. Jeddi, M. Ghaznavi and P. Chen, A novel polymer electrolyte to improve the cycle life of high-performance lithium–sulfur batteries, *J. Mater. Chem. A*, 2013, **1**, 2769–2772.

106 S. S. Zhang and D. T. Tran, how a gel polymer electrolyte affects performance of lithium/sulfur batteries, *Electrochim. Acta*, 2013, **114**, 296–302.

107 Y. Zhang, Y. Zhao and Z. Bakenov, A novel lithium/sulfur battery based on sulfur/graphene nanosheet composite cathode and gel polymer electrolyte, *Nanoscale Res. Lett.*, 2014, **9**, 137, DOI: 10.1186/1556-276X-9-137.

108 X. Wang, X. Hao, Y. Xia, Y. Liang, X. Xia and J. Tu, *J. Membr. Sci.*, 2019, **582**, 37–47.

109 Y. Meesala, A. Jena, H. Chang and R. S. Liu, Recent advancements in Li-ion conductors for all-solid-state Li-ion batteries, *ACS Energy Lett.*, 2017, **2**, 2734–2751.

110 X. Yu and A. Manthiram, Electrode–electrolyte interfaces in lithium–sulfur batteries with liquid or inorganic solid electrolytes, *Acc. Chem. Res.*, 2017, **50**, 2653–2660.

111 M. Zhu, Y. Wang, L. Long, X. Fu, G. Sui and X. Yang, an optimal carbon fiber interlayer integrated with bio-based gel polymer electrolyte enabling trapping-diffusion-conversion of polysulfides in lithium–sulfur batteries, *Chem. Eng.*, 2019, **370**, 1068–1076.

112 J. Yi, L. Chen, Y. Liu, H. Geng and L. Z. Fan, High capacity and superior cyclic performances of all-solid-state lithium–sulfur batteries enabled by a high-conductivity $Li_{10}S_nP_2S_{12}$ solid electrolyte, *ACS Appl. Mater. Interfaces*, 2019, **11**, 36774–36781.

113 R. C. Xu, X. H. Xia, S. H. Li, S. Z. Zhang, X. L. Wang and J. P. Tu, All-solid-state lithium–sulfur batteries based on a newly designed $Li_7P_{2.9}Mn_{0.1}S_{10.7}I_{0.3}$ superionic conductor, *J. Mater. Chem. A*, 2017, **5**, 6310–6317.

114 Y. Zhang, Y. Sun, L. Peng, J. Yang, H. Jia, Z. Zhang, B. Shan and J. Xie, Se as eutectic accelerator in sulfurized polyacrylonitrile for high performance all-solid-state lithium–sulfur battery, *Energy Storage Mater.*, 2019, **21**, 287–296.

115 F. Han, J. Yue, X. Fan, T. Gao, C. Luo, Z. Ma, L. Suo and C. Wang, High-performance all-solid-state lithium–sulfur battery enabled by a mixed-conductive Li_2S nanocomposite, *Nano Lett.*, 2016, **16**, 4521–4527.

116 M. Nagao, A. Hayashi and M. Tatsumisago, Sulfur–carbon composite electrode for all-solid-state Li/S battery with Li_2S–P_2S_5 solid electrolyte, *Electrochim. Acta*, 2011, **56**, 6055–6059.

117 M. Agostini, Y. Aihara, T. Yamada, B. Scrosati and J. Hassoun, A lithium–sulfur battery using a solid, glass-type P_2S_5–Li_2S electrolyte, *Solid State Ionics*, 2013, **244**, 48–51.

118 B. R. Shin and Y. S. Jung, All-solid-state rechargeable lithium batteries using $LiTi_2(PS4)_3$ cathode with Li_2S–P_2S_5 solid electrolyte, *J. Electrochem. Soc.*, 2014, **161**, A154.

119 H. Nagata and Y. Chikusa, Activation of sulfur active material in an all-solid-state lithium–sulfur battery, *J. Power Sources*, 2014, **263**, 141–144.

120 M. Nagao, A. Hayashi and M. Tatsumisago, Electrochemical performance of all-solid-state Li/S batteries with sulfur-based composite electrodes prepared by mechanical milling at high temperature, *Energy Technol.*, 2013, **1**, 186–192.

121 M. Nagao, A. Hayashi and M. Tatsumisago, High-capacity Li_2S–nanocarbon composite electrode for all-solid-state rechargeable lithium batteries, *J. Mater. Chem.*, 2012, **22**, 10015–10020.

122 T. Yamada, S. Ito, R. Omoda, T. Watanabe, Y. Aihara, M. Agostini, U. Ulissi, J. Hassoun and B. Scrosati, All solid-state lithium–sulfur battery using a glass-type P_2S_5–Li_2S electrolyte: Benefits on anode kinetics, *J. Electrochem. Soc.*, 2015, **162**, A646.

123 M. Nagao, A. Hayashi, M. Tatsumisago, T. Ichinose, T. Ozaki, Y. Togawa and S. Mori, Li_2S nanocomposites underlying high-capacity and cycling stability in all-solid-state lithium–sulfur batteries, *J. Power Sources*, 2015, **274**, 471–476.

124 Q. Wang, J. Jin, X. Wu, G. Ma, J. Yang and Z. Wen, A shuttle effect free lithium sulfur battery based on a hybrid electrolyte, *Phys. Chem. Chem. Phys.*, 2014, **16**, 21225–21229.

125 H. Nagata and Y. Chikusa, All-solid-state lithium–sulfur batteries using a conductive composite containing activated carbon and electroconductive polymers, *Chem. Lett.*, 2014, **43**, 1335–1336.

126 S. Kinoshita, K. Okuda, N. Machida, M. Naito and T. Sigematsu, All-solid-state lithium battery with sulfur/carbon composites as positive electrode materials, *Solid State Ionics*, 2014, **256**, 97–102.

127 M. Agostini, Y. Aihara, T. Yamada, B. Scrosati and J. A. Hassoun, A lithium–sulfur battery using a solid, glass-type P_2S_5–Li_2S electrolyte, *Solid State Ionics*, 2013, **244**, 48–51.

128 K. Suzuki, D. Kato, K. Hara, T. A. Yano, M. Hirayama, M. Hara and R. Kanno, Composite sulfur electrode prepared by high-temperature mechanical milling for use in an all-solid-state lithium–sulfur battery with a $Li_{3.25}Ge_{0.25}P_{0.75}S_4$ electrolyte, *Electrochim. Acta*, 2017, **258**, 110–115.

129 B. Huang, X. Yao, Z. Huang, Y. Guan, Y. Jin and X. Xu, Li_3PO_4-Doped $Li_7P_3S_{11}$ glass–ceramic electrolytes with enhanced lithium-ion conductivities and application in all-solid-state batteries, *J. Power Sources*, 2015, **284**, 206–211.

130 Y. Mo, S. P. Ong and G. Ceder, First principles study of the $Li_{10}GeP_2S_{12}$ lithium super ionic conductor material, *Chem. Mater.*, 2012, **24**, 15–17.

131 H. Nagata and Y. Chikusa, Activation of sulfur active material in an all-solid-state lithium–sulfur battery, *J. Power Sources*, 2014, **263**, 141–144.

132 M. Agostini, Y. Aihara, T. Yamada, B. Scrosati and J. A. Hassoun, A lithium–sulfur battery using a solid, glass-type P_2S_5–Li_2S electrolyte, *Solid State Ionics*, 2013, **244**, 48–51.

133 T. Yamada, S. Ito, R. Omoda, T. Watanabe, Y. Aihara, M. Agostini, U. Ulissi, J. Hassoun and B. Scrosati, All solid-state lithium–sulfur battery using a glass-type P_2S_5–Li_2S electrolyte: Benefits on anode kinetics, *J. Electrochem. Soc.*, 2015, **162**, A646.

134 M. Chen and S. Adams, High performance all-solid-state lithium/sulfur batteries using lithium argyrodite electrolyte, *J. Solid State Electron.*, 2015, **19**, 697–702.

135 E. Umeshbabu, B. Zheng, J. Zhu, H. Wang, Y. Li and Y. Yang, Stable cycling lithium–sulfur solid batteries with enhanced Li/$Li_{10}GeP_2S_{12}$ solid electrolyte interface stability, *ACS Appl. Mater. Interfaces*, 2019, **11**, 18436–18447.

136 R. R. Miao, J. Yang, X. J. Feng, H. Jia, J. L. Wang and Y. N. Nuli, Novel dual-salts electrolyte solution for dendrite-free lithium–metal based rechargeable batteries with high cycle reversibility, *J. Power Sources*, 2014, **271**, 291–297.

137 F. Wu, Q. Z. Zhu, R. J. Chen, N. Chen, Y. Chen, Y. S. Ye, J. Qiao and L. Li, Ionic liquid-based electrolyte with binary lithium salts for high performance lithium–sulfur batteries, *J. Power Sources*, 2015, **296**, 10–17.

138 G. Qiu and C. Sun, A quasi-solid composite electrolyte with dual salts for dendrite-free lithium metal batteries, *New J. Chem.*, 2020, **44**, 1817–1824.

139 H. Yao, K. Yan, W. Li, G. Zheng, D. Kong, Z. W. Seh and Y. Cui, Improved lithium–sulfur batteries with a conductive coating on the separator to prevent the accumulation of inactive S-related species at the cathode–separator interface, *Energy Environ. Sci.*, 2014, **7**, 3381–3390.

140 O. Eroglu, M. S. Kiai and H. Kizil, Glass fiber separator coated by boron doped anatase TiO_2 for high-rate Li–S battery, *Mater. Res. Bull.*, 2020, **8**, 110917.

141 S. S. Zhang, New finding on the role of $LiNO_3$ in lithium–sulfur battery, *J. Power Sources*, 2016, **322**, 99–105.

142 M. Barghamadi, A. S. Best, A. I. Bhatt, A. F. Hollenkamp, P. J. Mahon, M. Musameh and T. Rüther, Effect of $LiNO_3$ additive and pyrrolidinium ionic liquid on the solid electrolyte interphase in the lithium–sulfur battery, *J. Power Sources*, 2015, **295**, 212–220.

143 S. Xiong, K. Xie, Y. Diao and X. Hong, Characterization of the solid electrolyte interphase on lithium anode for preventing the shuttle mechanism in lithium–sulfur batteries, *J. Power Sources*, 2014, **246**, 840–845.

144 O. Eroglu, M. S. Kiai and H. Kizil, Performance enhancement of Li–S battery with the anatase nano structured Fe doped TiO_2 as a robust interlayer, *J. Alloys Compd.*, 2020, **16**, 155607.

145 N. Azimi, Z. Xue, I. Bloom, M. L. Gordin, D. Wang, T. Daniel, C. Takoudis and Z. Zhang, Understanding the effect of a fluorinated ether on the performance of lithium–sulfur batteries, *ACS Appl. Mater. Interfaces*, 2015, **7**, 9169–9177.

146 C. Zu, N. Azimi, Z. Zhang and A. Manthiram, Insight into lithium–metal anodes in lithium–sulfur batteries with a fluorinated ether electrolyte, *J. Mater. Chem. A*, 2015, **3**, 14864–14870.

147 N. Azimi, W. Weng, C. Takoudis and Z. Zhang, Improved performance of lithium–sulfur battery with fluorinated electrolyte, *Electrochem. Commun.*, 2013, **37**, 96–99.

148 N. Azimi, Z. Xue, N. D. Rago, C. Takoudis, M. L. Gordin, J. Song, D. Wang and Z. Zhang, Fluorinated electrolytes for Li–S battery: Suppressing the self-discharge with an electrolyte containing fluoroether solvent, *J. Electrochem. Soc.*, 2015, **162**, A64.

149 M. Liu, O. Meng, Z. Yang, X. Zhao and T. Liu, Ultra-long-term cycling stability of an integrated carbon–sulfur membrane with dual shuttle-inhibiting layers of graphene ''nets'' and a porous carbon skin, *Chem. Commun.*, 2018, **54**, 5090–5093.

150 Y. Yan, P. Zhang, Z. Qu, M. Tong, S. Zhao, Z. Li, M. Liu and Z. Lin, Carbon/sulfur aerogel with adequate mesoporous channels as robust polysulfide confinement matrix for highly stable lithium–sulfur battery, *Nano Lett.*, 2020, **20**, 7662–7669.

151 M. Liu, Z. Yang, H. Sun, C. Lai, X. Zhao, H. Peng and T. Liu, A hybrid carbon aerogel with both aligned and interconnected pores as interlayer for high-performance lithium–sulfur batteries, *Nano Res.*, 2016, **9**, 3735–3746.